Cíntia Leonora Semedo Veiga

Bachelor of Science in Chemical and Biochemical Engineering

Evaluation and prediction of the physical stability of amorphous drugs

Dissertation submitted for the degree of
Master in Chemical and Biochemical Engineering

Supervisor: Dr Luís Sousa, Hovione

Chairperson: Engineer Mário Fernando José Eusébio
Auxiliar Professor, NOVA School of Science and Tecnology

Opponent: Dr.Professor Maria Madalena Alves Campos de Sousa Dionísio
Associate Professor, NOVA School of Science and Tecnology

September, 2019

FACULDADE DE CIÊNCIAS E TECNOLOGIA
UNIVERSIDADE NOVA DE LISBOA

Cíntia Leonora Semedo Veiga

Bachelor of Science in Chemical and Biochemical

Evaluation and prediction of the physical stability of amorphous drugs

Dissertation submitted for the degree of
Master in Chemical and Biochemical Engineering

Adviser: Luís Sousa, PhD, Hovione

Examination Committee

ChairPerson	Mário Eusébio, Auxiliar Professor FCT-UNL
Opponent	Madalena Dionísio, Auxiliar Professor FCT-UNL

September, 2019

Evaluation and Prediction of the physical stability of amorphous drugs

Acknowledgements

After five years of this journey, I could not be more happy and thankful. All the working later and unslept hours, the tears, the smiles and the failures that turn to success later, it came to an end. To all who helped and participated in this journey, thank you.

To FCT NOVA for the excellent academic path during these five years. Also, to Hovione for the internship opportunity during this last semester at a company with such great values.

To Luís Sousa, my adviser, for his help, patience and guidance. For believing in my capacities and sharing with me during these six months his knowledge. It was a pleasure working with you.

To Professor Ana Aguiar Ricardo for her attention and help and also for the redirections during this journey and for the encouraging words and confidence through my work.

To all Hovione's students and collaborators for their support and sympathy, for the moments inside and outside Hovione, for all the histories and memories shared, but mostly, for making me feel part of a team.

To my best friends, Ana, Rita, Alexandra, Mariana Ferrão and Mariana Almeida for being the best group during these five years. For all our memories, the shared experiences, the smiles and tears. I am honoured to finish this cycle by your side and have you as best friends.

To my mother, father and sister for their support and love, for the values and education, and for being there every time that I needed.

This project was an excellent experience. To all and everyone, Thank you!

Abstract

The formulation of amorphous solids dispersion (ASDs) is a vanguard strategy used for the improvement of aqueous solubility and bioavailability of poorly water-soluble drugs. During formulation development it is very important to evaluate and predict long term physical stability of ASDs, particularly in supersaturated systems, since these forms are thermodynamically unstable. This project focuses not only on the evaluation of different thermodynamic and kinetics parameters that govern physical stability, but also on the development of a model that can effectively predict long term stability.

Six amorphous drugs and three amorphous solid dispersions were studied and parameters such as glass transition, fragility, relaxation and Kauzmann temperature were evaluated. A stability study was also conducted at 30 ºC to investigate potential correlations between the parameters and the onset of crystallization, which was monitored by X-ray Powder Diffraction (XRPD). Differential Scanning Calorimetry (DSC) and Dielectric Spectroscopy (DRS) were also used to determine all parameters abovementioned.

The study revealed that glass transition is not indicative of the physical stability of ASDs and, simultaneously, that the fragility index is not enough to rank the physical stability of amorphous drugs. Furthermore, a predictive model, that combines thermodynamic parameters with the kinetics of relaxation, was developed and showed to be a good indicator of physical stability. This approach was successfully employed allowing not only an early-stage assessment of physical stability, during the pre-formulation stage, but also an advanced analytical characterization.

Key-words: Amorphous solid dispersion; physical stability, Kauzmann temperature, relaxation, crystallization; glass transition temperature

Resumo

A formulação de dispersões sólidas amorfas (ASDs) é uma estratégia muito utilizada para o aumento da solubilidade e biodisponibilidade de fármacos pouco solúveis em água. Durante o desenvolvimento de formulações é necessário não só avaliar, mas também prever a estabilidade das dispersões sólidas amorfas a longo prazo, uma vez que estas formas são termodinamicamente instáveis, especialmente em sistemas supersaturados. Este projeto foca-se não só na avaliação dos parâmetros termodinâmicos e cinéticos que ditam a estabilidade física, mas ainda no desenvolvimento de um modelo capaz de prever de uma forma eficaz a estabilidade a longo prazo.

Para tal, foram estudados seis APIs (Active Pharmaceutical Ingredient) e três ASDs, os quais foram caracterizados e avaliados através de parâmetros como a temperatura de transição vítrea, a fragilidade, a relaxação e temperatura de Kauzmann. Posteriormente, foi realizado um estudo de estabilidade a 30ºC de modo a investigar potenciais correlações entre os parâmetros referidos anteriormente e inícios de cristalização, os quais foram monitorizados através de Calorimetria Diferencial de Varrimento (DSC) e Difração de Raios-X (XRPD). Adicionalmente, os parâmetros acima mencionados também foram caracterizados por Espectroscopia Dielétrica (DRS).

Primeiramente, este estudo revelou simultaneamente que a temperatura de transição vítrea e o índice de fragilidade não são correlacionáveis com a estabilidade física tanto dos APIs como das ASDs. Contrariamente, o modelo desenvolvido para a previsão da estabilidade mostrou ser um bom indicador de estabilidade. Este modelo, que considera tanto o efeito de parâmetros termodinâmicos como a cinética de relaxação, mostrou ser uma abordagem eficaz que permite não só uma previsão da estabilidade física durante a fase de pré-formulação como também permite uma caracterização analítica avançada.

Palavras chaves: dispersões sólidas amorfas, estabilidade física, temperatura de Kauzmann, relaxação, cristalização e temperatura de transição vítrea

Contents

List of figures

List of tables

Acronyms

API- Active Pharmaceutical Ingredient
ASD- Amorphous Solids Dispersion
DSC. Differential Scanning Calorimetry
XRPD- X-Ray Powder Diffraction
DRS- Dielectric Spectroscopy
GT- Gordon-Taylor
VTF- Vogel–Tammann–Fulcher
CRR- Cooperative rearranging regions
KWW- Kohlrausch-Williams-Watts

Nomenclature

T- temperature

G- free Gibbs energy

H- enthalpy

S- entropy

T_g- glass transition temperature

T_m- melting temperature

H_m- melting enthalpy

S_m- melting entropy

T_k- Kauzmann temperature

ρ -density

w- weight fraction

k- constant

m- fragility index

D- strength parameter

τ- relaxation time

τ_0- relaxation time at high temperature limit

B- free energy barrier opposing the rearrangements

S_{conf}- configurational Entropy

$c_{p,sc}$ - heat capacity of supercooled liquid

$c_{p,c}$- heat capacity of crystal

$c_{p,conf}$- configurational heat capacity

T_f- fictive temperature

T_2- temperature at where the configurational entropy is nill

A- constant

T_0- temperature where the structural relaxation time diverges

Φ- response function

t- time

β- stretch parameter

H_∞-maximum of enthalpy

$H_{relaxation}$- enthalpy of relaxation

T_a- annealing temperature

q- heating or cooling rate

R- ideal gas constant

$E_a(T_g)$- apparent activation energy at T_g

q_s- standard heating scan

m_{min}- fragility index of an unrestricted material

T_f^S -standard fictive temperature.

G_s- free energy necessary to create a surface for the particle

G_v- free energy involved in the transition of the liquid to the solid phase

d- distance between atomic layers in a crystal

θ - the incident angle

λ - wavelength of the incident X-ray beam

n – integer

ε- permittivity

C- capacitance

C_0- capacitance when the capacitor is empty

ε* - dielectric function

ω- angular frequency

ε'- real permittivity

ε''- imaginary permittivity

l-liquid

g-glass

sc-supercooled liquid

c- crystal

Motivation and Objectives

Over the years, the pharmaceutical industries have been providing drugs in various types of solid dosage forms [1-2]. The assurance of quality during the manufacturing process and the evaluation of drug performance, stability, and bioavailability of the final dosage form are critical and, as a result, the characterization of the properties of an active pharmaceutical ingredient (API) is an essential step in pre-formulation[3]. Solid state APIs can be delivered in an amorphous or crystalline form. However, in most cases, the crystalline form exhibits poor solubility and consequently poor bioavailability [4].

In order to improve the bioavailability of these forms of drugs, it is necessary to develop strategies to enhance their solubility, e.g., using pharmaceutical solid dosage forms in an amorphous state [5-6] Despite the advantages of this strategy in terms of solubility, amorphous solids are thermodynamically unstable, which means that they tend to crystallize with time. Hence, it is essential to predict the physical stability of these forms of drugs, which is influenced by factors, such as the relative humidity, thermodynamic properties, thermal history, preparation technique used and molecular mobility. Several studies have shown that molecular mobility is responsible for the chemical and physical instability of the amorphous phase [7–11].

In the present work, it is proposed to study not only the factors that influence the physical stability of amorphous solids dispersions but also possible correlations of drug physicochemical properties with the onset of recrystallization. These correlations can be very useful during the development stage, where physical stability is evaluated. Prior knowledge of these correlations and the prediction of stability, at these early stages, is very advantageous because it saves time, resources and materials otherwise spent in long-term stability studies.

To achieve this goal, the physical stability of six drugs was evaluated: indomethacin, itraconazole, nifedipine, sulindac, warfarin and cimetidine. The choice of the different drugs was made based on the similarity and differences between their thermodynamic properties, in order to obtain possible correlations with the onset of recrystallization. Therefore, the structure and the objectives of each chapter can be summed up as:

- **Chapter 1**, where a theoretical background is provided, not only to understand the main concepts involved in the discussion of this work, but also the choices made for the experimental work.
- **Chapter 2** summarizes the material used and describes the experimental procedures followed.
- **Chapter 3,** where the results are presented and discussed based on the theoretical background provided on Chapter 1.
- **Chapter 4,** where the conclusions are presented, as well as future work.

.

1 Introduction

The main bottleneck associated with the formulation of amorphous solids dispersions is their physical stability. Since these forms of drugs exhibit specific properties that allows improving the performance of pharmaceutical dosage forms, it is important to understand how these properties change with time in order to guarantee that the required effect is maintained. Therefore, this chapter will focus on the differences between the crystalline and amorphous state, the phenomenon of physical instability and its causes, as well as the state of art of the methods used for the prediction of physical stability.

1.1 Crystalline vs Amorphous state

The solid state differs from the liquid and gaseous states because it has lower mobility and its molecules occupy close positions in space [12]. Compounds in the solid state can appear in two different forms: crystalline or amorphous. The fundamental difference between amorphous and crystalline solids is the fact that, in the first one, the molecules are only arranged with a short-range order and there is no translational periodicity [1,13]. The opposite happens with the crystalline solids, where the crystal unit, which is composed by atoms, molecules or ions is arranged in a periodic 3D structure.

Another difference is that amorphous solids exhibit higher solubility, chemical reactivity and water vapor sorption compared to crystalline materials, as these forms are in a higher free energy state [1,13]. Hence, the amorphous solids tend to convert to the most stable and least energetic state, the crystalline state, losing the advantage of greater solubility.

The formulation of amorphous solids dispersions (ASDs) is a strategy used to enhance aqueous solubility and bioavailability of poorly soluble drugs. ASDs combine the solubility advantage of the high energy amorphous form with the improvements in dissolution rate that result from the polymeric counterpart. These solid dispersions are composed by an active pharmaceutical ingredient (API) and a water-soluble polymer that form an amorphous single phase [14]. The presence of the polymer not only inhibits the occurrence of crystallization, therefore promoting long-term stability, but also maintains drug supersaturation in the dissolution medium [15, 16].The addition of a surfactant in ASDs will also enhance the solubility.

Commonly, amorphous solids can be obtained either by fast cooling of a liquid melt to a certain temperature, where the liquid-like structure is frozen, or by solvent evaporation, as a result of the rapid increase in supersaturation. These solids are characterized by its structure with an extremely high viscosity [17]. Regarding large-scale production of amorphous materials, physical methods are the most used techniques, but these solids can also be prepared by chemical methods. The main difference between those is that in physical methods the composition of substances does not change during the transition, while in chemical methods some changes in chemical potential of the system may occur [18]. The most common processes of amorphization in physical methods are melt-quenching, spray drying, freeze-drying and mechanical milling. For chemical methods, gelation, precipitation by chemical reaction and dehydration of hydrate crystals are often used [18].

As the amorphous solids possess higher free energy, conversion into crystalline solids is expected in the course of time. However, crystalline solids can exhibit polymorphism, which is the ability of substance to exist in two or more crystalline phases [19-20]. Polymorphic forms differ from each other in their arrangements, which include not only the packing and orientation of the molecules but also their conformations. Because of these differences, polymorphic forms can exhibit different physicochemical characteristics that may impact pharmaceutical properties such as bioavailability [21–23].

Depending on the range of temperatures or pressures experimented, systems can undergo polymorphic transitions, i.e. conversion of one polymorphic form into another [24]. Polymorphic transitions can be classified as monotropic or enantiotropic. The system is considered monotropic when, at temperatures below the melting point, one polymorph is always more stable than the others. If over a certain range of temperatures and pressures a polymorphic form is stable while another polymorphic form is stable over a different range of temperatures, then the two polymorphs are categorized as enantiotropes [22], [24].

The free energy of conversion of the crystalline form into its amorphous counterpart (**Equation 1.1**), can be estimated by determining the differences in entropy and enthalpy between the two solid states, at the temperature of interest (*T*). It must be pointed out that the amorphous form can be present in a supercooled liquid or glassy state, as described in more detail in the following section. Since both enthalpy and entropy are functions of state, they do not depend on the path followed by the material to reach its present state, and thus, it is possible to calculate free energy differences (ΔG) by determining the partial changes in enthalpy (ΔH) and entropy (ΔS) during the conversion [25], as it can be seen in **Figure 1.1**.

$$\Delta G = \Delta H - T\Delta S$$

Equation 1.1

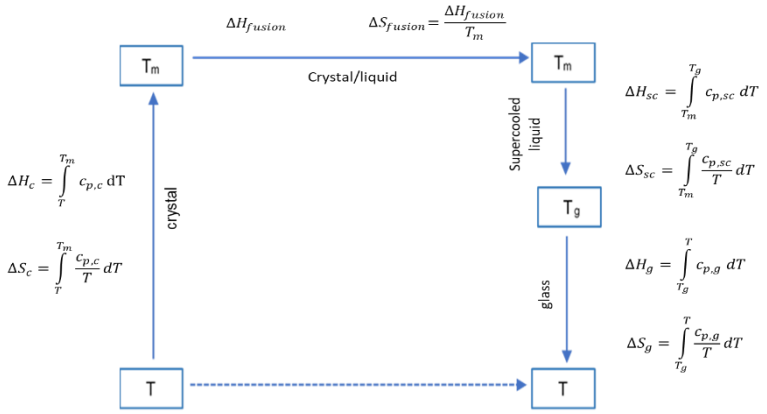

Figure 1.1- Determination of ΔS and ΔH during the conversion of a crystal to a glass at a certain temperature T.

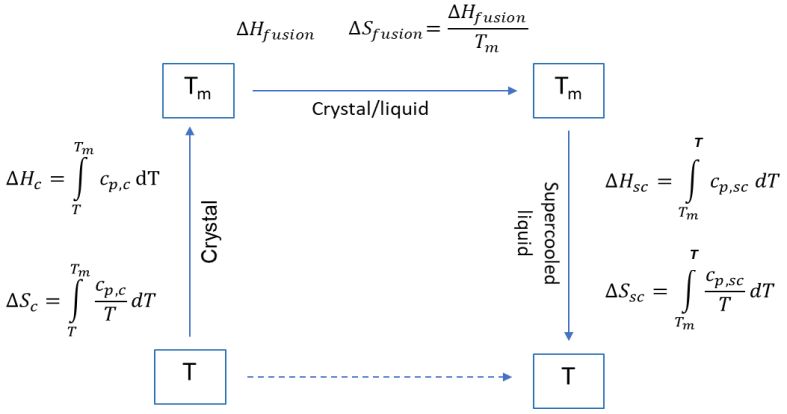

Figure 1.2- Determination of ΔS and ΔH during the conversion of a crystal to a supercooled liquid at a certain temperature T.

However, in the case of ASDs which are prepared by quench-melting of a physical mixture of polymer with crystalline API, it is necessary to consider other changes that occurs during the postulated path. One corresponds to the glass transition of the polymer and the other corresponds to the simultaneous melting and mixing of the API in the liquid polymer. This alternative path is shown in **Figure 1.3**for ASDs prepared with a polymer whose T_g is lower than the crystalline API melting temperature.

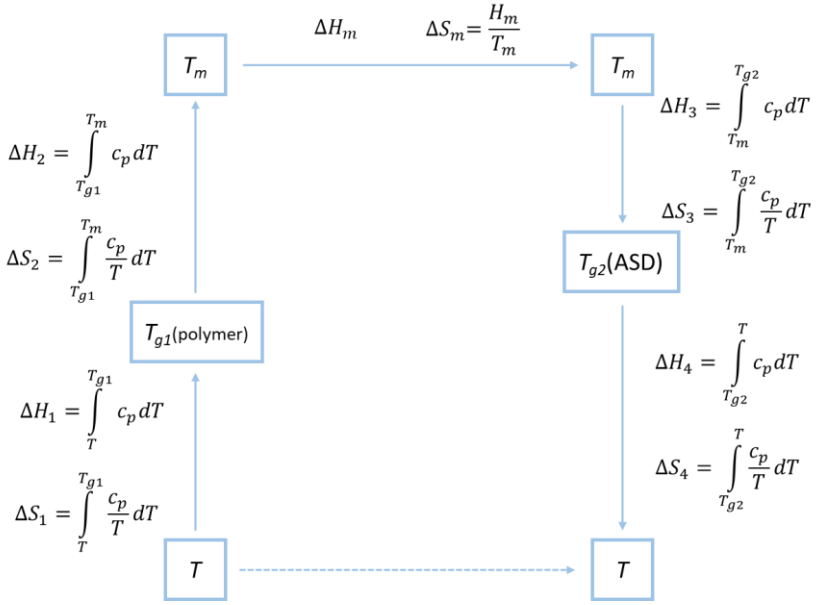

Figure 1.3- Determination of ΔS and ΔH during the conversion of a drug/polymer physical mixture to an ASD at a certain temperature T.

1.2 Glass transition

According to Ehrenfest, the phase transitions can be classified as first or second order, depending on the changes of state variables as entropy, enthalpy or volume, at the transition temperature [26]. While first order transitions exhibit a discontinuity in the first derivative of the chemical potential, with respect to temperature, the second order transitions exhibit a discontinuity in the second derivative. Therefore, in first order transitions the change in heat capacity is infinite since the change of enthalpy is greater than the change of temperature, which thermodynamically means that these transitions involve latent heat, e.g melting or crystallisation [26]. On the other hand, in second order transitions the heat capacity varies discontinuously at the transition but does not tend to infinite at this point. An example of this type of transition is vitrification or glass transition.

During the cooling of a liquid at a high temperatures two types of transitions could occur. According to **Figure 1.4**, if the liquid is slowly cooled below to its melting temperature, then crystallisation takes place (first order transition). However, if the rate of cooling is fast enough it is possible to avoid crystallisation and the system goes to a metastable phase known as supercooled liquid. Upon further cooling, the viscosity of the supercooled liquid increases such that the molecular motions slow down, and equilibrium can no longer be maintained resulting in a formation of an unstable glassy material. This change happens at glass transition temperature (T_g) and it is considered a second order transition [27]. Conventionally, the glass transition temperature is considered as the temperature where the viscosity reaches a value of approximately 10^{12} Pa.s or where the structural relaxation time is around 100 s [1]. This value of relaxation

time was obtained considering the viscosity value of 10^{12} Pa.s and the shear modulus at infinity frequency, as described by the Maxwell relationship in **Equation 1.2 .**

$$\eta = \tau * G_{\infty}$$

Equation 1.2

Where,

- η is the viscosity;
- τ is the relaxation time;

G_{∞} is the shear modulus at infinity frequency

Furthermore, it is important to take into account that the glass transition is a kinetic phenomenon, which means that the glass transition temperature depends on the cooling rate; the faster the cooling rate, the greater is T_g [1].

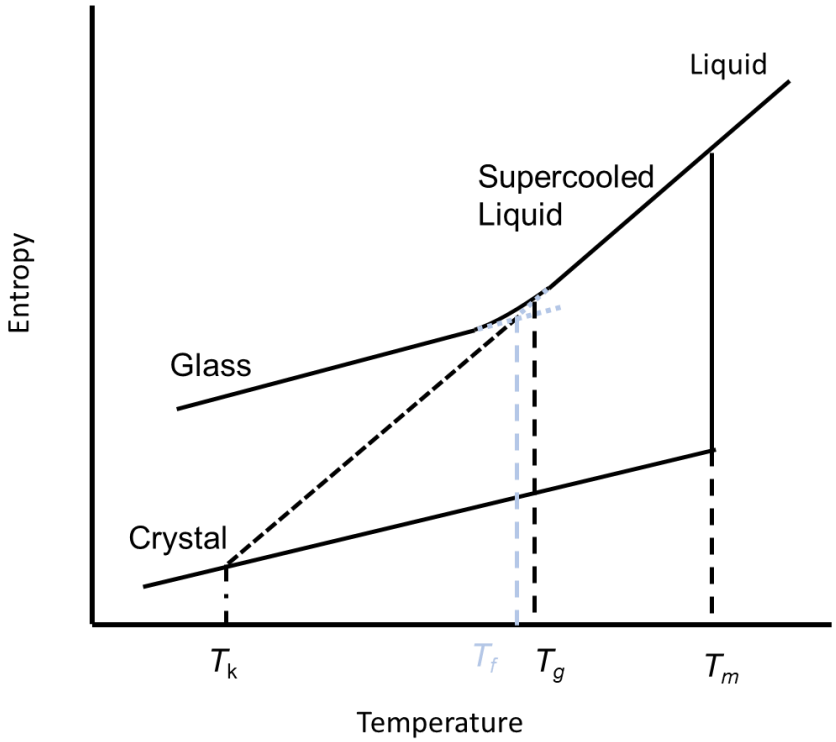

Figure 1.4- Variation of entropy with temperature [1].

It is important to mention that experimentally the glass transition shows a lower limit known as the Kauzmann temperature (T_k) as shown in **Figure 1.4**.Upon continuous cooling of a liquid, there will be a temperature where the entropy of the liquid is equal to that of the crystalline solid, and consequently, the

entropy of a liquid is lower than the crystalline counterpart, which thermodynamically corresponds to a paradox [27- 28]. This temperature is defined as the Kauzmann temperature.

In the case of ASDs, the glass transition temperature depends on the drug/polymer composition and can be predicted by Gordon-Taylor (GT) equation. This equation (**Equation 1.3**) is used in the case of ideal mixing between the API and the polymer [30].

$$T_{g,mix} = \frac{w_A . T_{g,A} + k . w_B T_{g,B}}{w_A + k . w_B}$$

Equation 1.3

$$k = \frac{\rho_A T_{.gB}}{\rho_B T_{g,B}}$$

Equation 1.4

Where

- T_{gA} e T_{gB} correspond to the glass transition temperature of the component A and B, respectively;
- w_A and w_B represent the weight fraction of the component A and B, respectively;
- k is a constant;
- ρ_A and ρ_B is the densitiy of the component A and B

1.3 Structural relaxation and molecular mobility

The physical properties of amorphous glassy materials are very different when compared to crystalline solids. However, with time, these properties will change due to structural or enthalpic relaxation towards an equilibrium state. This process, also called physical aging, is observed when the amorphous form loses its excess energy and no recrystallization occurs [29]. This behaviour suggests that below T_g molecular mobility still exists, and therefore, the time scale of this process depends on how close the temperature is from T_g: if the temperature is near T_g, structural relaxation will be faster.

The molecular dynamics of amorphous solids is responsible for different types of relaxations that can occur near and below T_g. Generally, there are two types of motions: α – relaxations that are associated to the global mobility of the molecule and are characterized by its cooperative behaviour; and sub-α relaxations β, γ, δ that are linked to local mobility and result from the rotation of functional groups [30-31]. While α-relaxation is associated to glass transition, the secondary relaxations occur at temperatures lower than T_g , but they are still active above this temperature [33].

The molecular mobility of a material is temperature dependent since an increase in temperature conducts to an increase in free volume. This change can be described according to models such as the

Williams–Landel–Ferry equation (WLF) [1]. For some supercooled liquids the dependence of molecular motions on temperature is characterized by being an activate process, which means that the mobility can be described by the Arrhenius equation [32-35]. However, for many supercooled liquids a deviation from Arrhenius behaviour was detected. This nonconformity behaviour is characteristic of fragile liquids and is explained by the heterogeneity in structure which is inherent to disordered systems [41]. At temperatures close to T_g, the properties of glass forming liquids, such as shear viscosity or relaxation time, can exhibit different behaviors that are classified as strong or fragile. In a strong liquid, the viscosity or relaxation time follows an Arrhenius behavior with temperature, which means that its structure does not change significantly around T_g; the opposite happens to fragile liquids [36-38]. During cooling, the change in liquid dynamics can be measured in terms of the fragility index, *m*, or the strength parameter, D, that are parameters used in the Vogel–Tammann–Fulcher (VTF) model, which will be presented later in this chapter. For most pharmaceutical compounds, the fragility index takes values between 16 and 200. For values of m≈200 and D <10 the liquid is fragile; for m≈16 and D > 30, the liquid is strong, and between this range is moderately fragile [39].

Molecular mobility in amorphous solids can be evaluated by means of the structural relaxation time (τ). Since glass formation results in an excess of energy which is kinetically trapped, as the system falls out of equilibrium, an accurate method to assess the relaxation time involves determining the excess of entropy [40]. According to Adam Gibbs Model, **Equation 1.5** , the structural relaxation time of a supercooled liquid is govern by the configurational entropy which determines the size of cooperatively rearranging regions (CRR) [28,40]. These regions are defined as the smallest molecular groups that can relax to new configurations, independently of the environment. As a result, their size is temperature dependent in a way that the decrease in temperature results in an increase in CRR size and a decrease in configurational entropy [28, 40, 41].

$$\tau(T) = \tau_0 \exp\left(\frac{B}{TS_{conf}(T)}\right)$$

Equation 1.5

The parameter τ_0 represents the relaxation time at the high temperature limit and the value of B represents the free energy barrier opposing the rearrangements. The configurational entropy, S_{conf}, can be easily estimated by the configurational heat capacity, which corresponds to the difference between the heat capacities of the liquid and the crystal (**Equation 1.6**) [43].

$$S_{conf}(T) = \int_{T_k}^{T} \frac{c_{p,conf}}{T} dT = \int_{T_k}^{T} \frac{c_{p,l} - c_{p,c}}{T} dT$$

Equation 1.6

It is important to note that glass transition is not an equilibrium state, thus, once the glass is formed it will always relax toward the equilibrium. This means that configurational entropy is not only temperature but also time dependent. Therefore, the thermodynamics properties of relaxing glasses can be expressed in terms of another parameter, which is the fictive temperature. This temperature is defined as the temperature at which the system under investigation has the same thermodynamics properties as its equilibrium state at that temperature and time [17, 37, 43, 44]. Rearranging **Equation 1.6**, it is possible to express the configurational entropy in terms of this fictive temperature (**Equation 1.7**), and obtain the relaxation time with **Equation 1.8**.

$$S_{conf}(T_f) = \int_{T_k}^{T_f} \frac{\Delta c_{p,conf}(T)}{T} dT$$

Equation 1.7

$$\tau(T, T_f) = \tau_0 \exp\left(\frac{B}{T S_{conf}(T_f)}\right)$$

Equation 1.8

For many inorganic glasses, a hyperbolic correlation describes the variation of $\Delta c_{p,conf}$ [29] with temperature, as in **Equation 1.9**. This expression is used with **Equations 1.8** and **1.9** to obtain **Equation 1.10**, which is used to determine the relaxation time.

$$\Delta c_p = \frac{A T_2}{T}$$

Equation 1.9

Where

- T_2 is the temperature where the configurational entropy is zero.
- A is a constant.

$$\tau(T, T_f) = \tau_0 \exp\left(\frac{B}{T\left(1 - \frac{T_2}{T_f}\right)}\right)$$

Equation 1.10

Structural relaxation dependence on temperature can also be described by the empirical Vogel-Fulcher-Tammann (VTF) law, **Equation 1.11**. In this equation, T_0, corresponds to the temperature where

the structural relaxation time diverges. In practice, T_0 corresponds to the temperature where the molecular mobility of glasses is practically nil, and therefore, correlates well with the Kauzmann temperature [46]. As mentioned before, D represents the strength parameter.

$$\tau(T) = \tau_0 \exp\left(\frac{DT_0}{T - T_0}\right)$$

Equation 1.11

Another characteristic of the behavior of viscous liquids close to T_g is the non-exponential relaxation in response to a perturbation in the system. An approach to estimate molecular mobility, based on relaxation times, involves the empirical Kohlrausch-Williams-Watts (KWW) equation (**Equation 1.12**), which describes the temporal behavior of the response function $\emptyset(t)$. This equation contains the stretch parameter, β, that describes the distribution of the relaxation times and varies between 0 and 1 [44] [47]. Since the KWW equation predicts a stretched exponential decay of the change in properties, it can be applied to the variation of the enthalpy of relaxation with time. Therefore, this variation can be also expressed by **Equation 1.13**, where the parameter ΔH_∞ represents the maximum enthalpy of relaxation of the glass. This maximum enthalpy can be estimated by **Equation 1.14** [47].

$$\emptyset(t) = \exp\left(-\left(\frac{t}{\tau}\right)^{\beta}\right)$$

Equation 1.12

$$\emptyset(t) = 1 - \frac{\Delta H_{relaxation}}{\Delta H_\infty}$$

Equation 1.13

$$\Delta H_\infty = \Delta c_p(T_g).(T_g - T_a)$$

Equation 1.14

Where,

- $\Delta c_p(T_g)$ is the heat capacity change at T_g;
- T_a is the annealing temperature

As mentioned previously, the deviation from the Arrhenius behavior for supercooled liquids and glasses can be quantified by means of the fragility index, which is an indicator of how fast the molecules lose their degrees of freedom. In the literature, the estimation of this index is described by different methods that sometimes lead to very different values [4, 9, 44]. The estimation of the ‘‘thermodynamic’’ fragility (m) is a simple approach which considers the changes in thermal properties at T_g (**Equation 1.15**). A fragile

glass former presents large changes in its thermal properties around T_g, while the strong glass former shows smaller changes.

$$m = \frac{\Delta c_{p,conf}}{\Delta c_p}\Big|T_g$$

Equation 1.15

Where, $\Delta c_{p,conf}$ is the difference in heat capacity between the supercooled liquid and the crystal, and Δc_p is the heat capacity change at T_g

Another method to estimate the fragility involves determining the strength parameter, D, that appears on the VTF equation [48]. Considering the variation of the structural relaxation time with temperature, at glass transition, the fragility index can be determined by **Equation 1.16**.

$$m = \frac{D\left(\frac{T_0}{T_g}\right)}{ln10\left(1-\frac{T_0}{T_g}\right)^2}$$

Equation 1.16

Alternatively, considering the dependence of T_g on the heating or cooling rate, q, it is possible to estimate the fragility index by determining an apparent activation energy based on DSC measurements. Using this method, the parameters m and D can be calculated by the following equations [31, 33, 36]:

$$\frac{d(lnq)}{d\left(\frac{1}{T_g}\right)} = -\frac{\Delta E_{a_{T_g}}}{R}$$

Equation 1.17

$$m = \frac{dlog\tau}{d\left(\frac{T_g}{T}\right)}\Big|T_g = \frac{1}{ln10}\frac{\Delta E_{a_{T_g}}}{R}$$

Equation 1.18

$$D = ln10\frac{m_{min}^2}{(m-m_{min})}$$

Equation 1.19

Where m_{min} represents the relaxation of an unrestricted material and $\Delta E_{a_{T_g}}$ is the activation energy at T_g. Considering that at T_g, $\tau = 100$ s, m_{min} can be calculated with the following equation:

$$m_{min} = \log\left(\frac{\tau(T_g)}{\tau_0}\right) = \log\left(\frac{100}{10^{-14}}\right) = 16$$

Equation 1.20

An alternative method can be used to determine the fragility using the fictive temperature instead of the glass transition temperature. In this case, the effect of different cooling rates, that lead to different extends of energy entrapment, on the fictive temperature is evaluated. The same heating rate is used for monitoring the differences in fictive temperature. The heating rate is designated the standard heating scan (q_s) [37].

$$\log\left(\frac{q}{q_s}\right) = m - m\frac{T_f^s}{T_f}$$

Equation 1.21

Where,

- q is the cooling rate,
- q_s is standard heating rate
- T_f^s is the standard fictive temperature.

1.4 Crystallization

Crystallization corresponds to the process that leads to the formation of a crystalline solid. Commonly, crystals are obtained by crystallization from solution, where the supersaturation is the driving force for precipitation [49]. Supersaturation can be created by a change in temperature, solvent evaporation, a change in pH or chemical reaction. Since a supersaturated system is a non-equilibrium state, which means that the concentration of the solute exceeds its equilibrium concentration, the system will tend to its lower energy state, with time, and crystallization will occur [17, 48, 49, 51].

The principles that guide the crystallization process are based on the classical nucleation theory (CNT) for homogeneous nucleation. According to this theory, crystallization occurs in two steps: a nucleation step followed by crystal growth [1, 17]. For nucleation to occur – the formation of various crystal nuclei - it is important to overcome the energetic barrier that is described in **Equation 1.22**. The process is classified as primary nucleation, when it occurs without the presence of crystals, or secondary nucleation when the formation of a nuclei occurs in the presence of crystals [1, 17]

$$\Delta G = \Delta G_v + \Delta G_s$$

Equation 1.22

Where,

- ΔG_s corresponds to the free energy necessary to create a surface for the particle, J/mol
- ΔG_v corresponds to the free energy involved in the transition of the liquid to the solid phase, J/mol

Once nucleation has occurred, crystal growth takes place. This step includes a mass transfer process by diffusion and adsorption at the crystal surface. Therefore, it is possible to conclude that crystallization not only is a thermodynamic process but also a kinetic one. At lower temperatures, the crystallization process is explained by thermodynamic factors since the driving force for recrystallization is larger, while at higher temperatures the kinetic factors are more relevant, as the molecular mobility increases and crystallization is faster [1]. Although many theories try to explain the structural relaxation of the amorphous forms and how its molecular mobility varies with temperature, few are the models found in the literature that try to predict the onset of crystallization [52].

1.5 Characterization techniques

1.5.1 Differential Scanning Calorimetry (DSC)

Differential scanning calorimetry (DSC) is a thermal analysis technique that measures the heat flow associated with physical and chemical changes as a function of temperature or time. The physical and chemical changes are associated to endothermic and exothermic processes or changes in heat capacity [53].

The DSC measures the heat flow from/to the sample relatively to a reference. The equipment is composed by a furnace that contains two pans: the reference pan, that is empty, and the pan that contains the sample. When the sample is heated, the heat flow ($\frac{dq}{dt}$) is measured and converted to heat capacity (c_p) as shown in **Equation 1.23**.

$$\frac{dq}{dt} = c_p \frac{dT}{dt}$$

Equation 1.23

Where,

- $\frac{dT}{dt}$ corresponds to the heating rate.

However, conventional DSC has limitations since multiple transitions can occur simultaneously. For example, at the glass transition temperature, the change in reversible heat capacity occurs at the same time as the enthalpic relaxation recovery. As conventional DSC measures the total heat flow from all thermal events, the results sometimes can be very confusing and difficult to analyze. To overcome the limitations of conventional DSC, it is possible to modulate the heat flow signal and separate the reversible from the non-

reversible signals. This method uses a different heating program where a sinusoidal modulation is overlaid to the conventional linear heating or cooling ramps [53]. According to **Equation 1.24**, in modulated DSC the total heat flow has two components. On the right-hand side of the equation ($f(T,t)$), the non-reversible heat flow or kinetic component, provides information on the kinetic processes; on the left ($c_p\beta$), the reversible heat flow or heat capacity component, contains information on heat capacity changes.

$$\frac{dQ}{dt} = c_p\beta + f(T,t)$$

Equation 1.24

Generally, in DSC experiments an inert atmosphere, usually nitrogen, is necessary to provide an efficient heat transfer, to help the cell cooling and to remove the moisture or oxygen which may accumulate and damage the cell over time [54].

1.5.2 X-ray powder diffraction (XRPD)

X-ray powder diffraction is a technique used to identify crystalline materials and provides information on unit cell dimensions. Hence, this technique is widely used to identify and quantify the presence of crystallinity in amorphous systems [55].

This technique is based on the occurrence of diffraction of the electromagnetic radiation upon interaction with the atoms of a material. When the diffraction conditions satisfy Bragg's law (**Equation 1.25**), the interaction produces constructive interference. This law relates the wavelength of electromagnetic radiation to the diffraction angle and the lattice spacing in a crystalline sample.

$$2(d\sin\theta) = n\,\lambda$$

Equation 1.25

Where,

- d is the distance between atomic layers in a crystal;
- θ is the incident angle;
- λ is the wavelength of the incident X-ray beam;
- n is an integer.

Since the powder material is prepared with a random orientation, by scanning the sample through a range of 2θ angles, all possible diffraction directions of the lattice are then collected. As every crystalline solid will have a unique pattern of d-spacings, XRPD is a standard technique in the characterization of pharmaceutical crystalline materials. Amorphous materials, on the other hand, do not possess long-range periodicity and atoms are randomly distributed in space. Therefore, X-ray diffraction does not produce

constructive interference and, hence no diffraction peaks are detected in the diffractograms. Amorphous materials only show a broad halo typical of short-range order.

1.5.3 Dielectric spectroscopy (DRS)

Dielectric spectroscopy is a technique which allows a detailed study of the molecular dynamics and the electric behavior of a material, not only across a large range of temperatures, but also with time. This method is based on the analysis of the polarization effect of a material as a response to the application of an electric field in the sample [35, 45, 53, 55]. The mechanisms of polarization can be divided into two groups: induced polarization due to charge migration, which includes the electronic and atomic polarization, and the orientational polarization due to alignment of permanent dipoles [45, 53].

In this technique the dielectric material is introduced in a capacitor which is composed by two conductive electrodes. The extent of polarization is quantified by means of the permittivity (ε) of a material to the electric field, **Equation 1.26**.

$$\varepsilon = \frac{C}{C_0}$$

Equation 1.26

where,

- C corresponds to the capacitance of the capacitor and C_0 when it is empty.

If an alternating voltage is applied to the capacitor, the electric field can be described in a complex form, and consequently the dielectric permittivity too. As it can be seen in **Equation 1.27**, the dielectric function, $\varepsilon^*(\omega)$, contains a real, $\varepsilon'(\omega)$, and an imaginary permittivity, $i\varepsilon''(\omega)$. While the real part represents the effect of polarization as function of frequency, the imaginary part represents the dielectric loss that results from molecular motions no longer following the orientation of the alternation of the electric field.

$$\varepsilon^*(\omega) = \varepsilon'(\omega) - i\varepsilon''(\omega)$$

Equation 1.27

The fact that the polarization no longer follows the alternate current field is reflected by a decay in the real permittivity and a peak in the dielectric loss at a certain frequency, which can be shifted by increasing the temperature. The detection of this peak identifies the dielectric relaxation mechanism that can be detected over a different range of temperatures. Thus, with this technique it is possible to access the different mechanisms of relaxation according not only to temperature but also with time

2 Materials and Methods

2.1 Materials

Six drugs were chosen for the studies presented herein. Indomethacin, nifedipine, cimetidine, warfarin and sulindac were purchased from Sigma-Aldrich (St. Louis, MO, USA) while itraconazole from Fagron (Spain, SP). The polymer PVP K29/32 was purchased from Ashland (Covington, KY, USA) and Eudragit E PO was obtained from Evonik Industries (Essen, Germany).

2.2 Methods

2.2.1 API characterization in the DSC

To characterize the selected APIs and ASDs, their thermal properties were evaluated in the crystalline and amorphous states. Thermal measurements were performed in a Discovery DSC 250 (TA Instruments, New Castle, DE) and 4 to 5 mg of each sample were placed in Tzero aluminum pans (TA Instruments). Typically, this type of pans is used when it is necessary to measure heat capacities as the heat transfer area is larger. To obtain accurate results, temperature and enthalpy calibrations and verifications were done routinely using indium. For heat capacity calibrations, sapphire was used. Samples were equilibrated at 25 ºC, in the DSC. The temperature modulation amplitude was 1ºC using a modulation period of 60 s. Samples were heated at 2ºC/min until complete melting. Since all APIs have a T_g above 0ºC, to form the amorphous glass, a fast cooling rate was applied after melting, by equilibrating the system to 0 ºC. Afterwards, the samples were heated again at 2ºC/min, above their glass transition temperature. Nitrogen was used as purge gas with a flowrate of 50 mL/min.

2.2.2 Evaluation of the impact of different cooling rates on T_g

Each API was analyzed in the Discovery DSC 250 to evaluate the impact of different cooling rates on the glass transition phenomenon. After calibration and verification with indium, 4 to 5 mg of sample were loaded into a Tzero aluminum pan and the program used in section 2.2.1 was followed to generate the

amorphous form. Then, the melt-quenched samples were subjected to cycles of cooling and heating, from 0ºC to a temperature above T_g, and vice-versa. The heating rate was always equal to 2ºC/min and the cooling rates varied between 25 to 2ºC/min to 0ºC. All the measurements were conducted with a nitrogen purge flowrate of 50 mL/min.

2.2.3 Preliminary stability studies in the DSC

In order to evaluate the drugs' tendency of crystallization, experiments were conducted in the Discovery DSC 250 to evaluate the onset of crystallization at high temperatures, for a maximum period of 12 hours. After calibration and verification with indium, 4 to 5 mg of sample were loaded into a Tzero aluminum pan and heated up to the melting temperature, at 2 ºC/min, using a modulation amplitude of 1ºC and a period of 60 s. Then, the samples were equilibrated at 120ºC and kept at this temperature for 12 hours, with the exception of warfarin that was kept at 100ºC for the same period of time. Past this time, the samples were heated again at 2ºC/min up to the melting point. All the measurements were conducted with a nitrogen purge flowrate of 50 mL/min.

2.2.4 Relaxation studies in the DSC

To evaluate the molecular mobility of glasses as a function of relaxation time, enthalpy recovery experiments were carried out in the Discovery DSC 250, for each API. After calibration and verification with indium, 4 to 5 mg of sample were loaded into a Tzero aluminum pan and heated up to the melting temperature, at 2 ºC/min, using a modulation amplitude of 1ºC and a period of 60 s. Afterwards, the samples were equilibrated at 0ºC and reheated at a rate of 2ºC/min up to 20ºC above the glass transition temperature. The the samples were annealed at 30ºC for different periods of time: 2, 4, 6 and 12 hours. After each isothermal step, the samples were equilibrated at 0ºC and followed by a reheating step at 2ºC/min up to 20ºC above T_g. After the last annealing step, samples were heated at 2ºC/min up to melting point. All the measurements were conducted with a nitrogen purge flowrate of 50 mL/min.

2.2.5 Preparation of amorphous glasses for the stability study

First, binary mixtures of crystalline nifedipine and two different polymers, PVP K29/32 and Eudragit EPO, were prepared. Nifedipine/Eudragit EPO mixtures were prepared at 60:40 and 80:20 w:w ratios, while a single nifedipine/PVP K29/32 mixture was prepared at 80:20 w:w ratio. During the preparation, the two components were successively added in equal proportions and then mixed with a mortar and a pestle. The physical mixture with PVP 29/32 is designated by physical mixture A and the mixtures with Eudragit EPO by physical mixtures B (80:20) and C (60:40).

The binary mixtures and individual APIs were then made amorphous by melt-quenching in two different ways. For samples analyzed by XRPD, amorphous glasses were prepared in aluminum foil. On the other hand, samples to be analyzed in the DSC were prepared inside the Tzero aluminum pans. All crystalline APIs and the physical mixtures of API/polymer were melted in a hot plate, where the temperature control was assured with syltherm. After melting, the samples were cooled in a freezer and kept for 30 minutes at -20 ºC. An additional sample of cimetidine was prepared by solvent evaporation, using methanol as solvent. In total, 24 samples were prepared, for each API and ASD: 12 for analysis by XRPD and the other 12 by DSC.

2.2.6 Long-term stability study

The stability study was initiated after storing the samples at 30ºC and 0% RH in an oven. DSC and XRPD measurements were performed immediately after preparation and at time-points 1, 3 (or 4) and 7 days, and, afterwards, every week up to 3 months.

The X-ray powder diffractograms for the crystalline and amorphous APIs were obtained in a Empyrean II diffractometer with a PIXcel1D detector, using a Cu Kα radiation source, a voltage of 45 kV and a current of 40 mA. The samples were prepared in a zero-background sample holder and the measurements were performed in a scan range from 2-50 º 2Θ, with a scanning rate of 0.328º/s and an acquisition time of 100 s/step. Stability samples prepared in aluminium foil were wrapped around the sample holder disk and held in place with the metal rim.

For samples analysed in the Discovery DSC 250, a modulated heating ramp was performed at a heating rate of 2ºC/min until T_m. The modulation amplitude was 1ºC and the period was 60 s.

2.2.7 API characterization by dielectric spectroscopy

Dielectric spectroscopy studies were conducted in an N-Alpha Analyzer (Novocontrol GmbH), in order to characterize each API and its molecular mobility over a wide range of temperatures. Samples were loaded between two gold-plated electrodes with a diameter of 10 mm, which were separated by two silica spacers of 50 µm of thickness. Measurements were performed in a frequency range between 10^{-1} to 10^{6} Hz. Each sample was heated slightly above T_m at a rate of 10ºC/min and kept at the maximum temperature for 5 minutes to ensure complete melting. Afterwards, the samples were cooled, and the dielectric spectra collected isothermally until a temperature of -120ºC. This cooling procedure was conducted in different steps: from -120 ºC to 30ºC, in steps of 5ºC; from 32 ºC to 80ºC, in steps of 2ºC, and the last temperature range in steps of 5ºC. These measurements were only performed for indomethacin, nifedipine and sulindac.

2.2.7.1 Analysis of the dielectric spectra

The dielectric spectra were analysed considering the imaginary part of permittivity as a function of temperature, at a certain frequency. In this isochronal representation, the relaxation mechanisms were identified as peaks in the dielectric loss function. Thus, for each frequency, the maximum temperature peaks were identified, as shown in **Figure 2.1**. Depending on the type of relaxation, the collected data was fitted to the VTF model (**Equation 2.1**), in the case of α- relaxations, and fitted to **Equation 2.5**, in the case of sub α- relaxations.

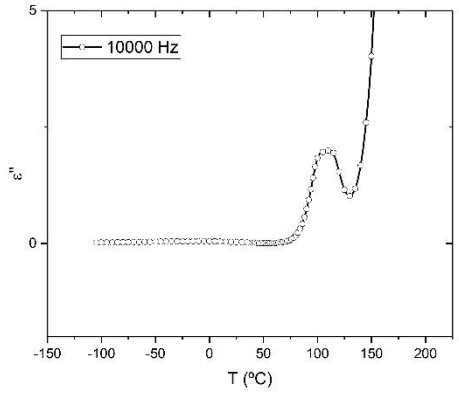

Figure 2.1- Analysis of the dielectric spectra

$$\log(\tau) = P_1 + \left(\frac{-P_2}{\frac{1000}{T_{max}} - P_3}\right)$$

Equation 2.1

Where

- P_1, P_2 and P_3 are the fitting parameters.

$$\tau_0 = 10^{P_1}$$

Equation 2.2

$$B = P_2 * \ln(10)$$

Equation 2.3

$$T_0 = P_3$$

Equation 2.4

$$\log(\tau) = A_1 * \frac{1000}{T_{max}} + A_2$$

Equation 2.5

Where,

- A_1 and A_2 are the fitting parameters.

$$E_a = -A_1 * R * \ln(10)$$

Equation 2.6

Where,

- R is the ideal gas constant.

$$\tau = \frac{1}{2 * \pi * \omega}$$

Equation 2.7

Where,

- ω is the angular frequency.

The glass transition temperature was determined by taking the temperature value corresponding to a relaxation time of 100s. In addition, the apparent activation energy, $E_a(T_g)$, and the fragility index, m, were determined, according to **Equation 2.8** and **Equation 2.9**, respectively.

$$E_a(T_g) = \frac{R.B}{\left(1 - \frac{T_0}{T_g}^2\right)}$$

Equation 2.8

$$m = \frac{E_a(T_g)}{ln10.R.T_g}$$

Equation 2.9

Where,

- R is the ideal gas constant;
- T_0 is the temperature where the configurational entropy is nil;
- B is the fitting parameter of the VTF equation

2.2.8 Determination of Kauzmann Temperature, $\Delta S(T)$, $\Delta H(T)$ and $\Delta G(T)$

Since it is difficult to measure experimentally the Kauzmann temperature (T_k) - glass transition or crystallization phenomena will occur above that temperature - one approach to estimate T_k is considering that at this temperature the difference between the entropy of the liquid and the crystal is zero. **Equation 2.10**. can be used to determine $\Delta S_{c\text{-}sc}$.

The heat capacity terms in that equation were obtained by fitting the reversible heat capacity data, obtained in the DSC, to a linear function of temperature, as shown in **Equation 2.11** and **Equation 2.12** For temperatures below the glass transition temperature, the heat capacity data for the supercooled liquid was extrapolated from the fitting equation obtained above T_g.

$$\Delta S(T)_{c-sc} = \int_{T}^{T_m} \frac{c_{p,c}}{T} dT + \frac{\Delta H_m}{T_m} + \int_{T_m}^{T} \frac{c_{p,Sc}}{T} dT$$

Equation 2.10

Where,

- $c_{p,c}$ is the heat capacity of the crystal;
- $c_{p,sc}$ is the heat capacity of the supercooled liquid;

$$c_{p,c} = C_0 + C_1.T$$

Equation 2.11

$$c_{p,sc} = B_0 + B_1.T$$

Equation 2.12

Where,

- C_0, C_1, B_0 and B_1 are the fitting parameters.

Thus, after replacing the heat capacity terms in **Equation 2.10** with the linear expressions of c_p and integrating over a range of temperatures, the following equation gives the change in entropy that occurs for the conversion of a crystal to its supercooled liquid counterpart. The Kauzmann temperature will then correspond to the temperature at which **Equation 2.13** equals 0.

$$\Delta S(T)_{c-sc} = C_1.(T_m - T) + C_0.\ln\left(\frac{T_m}{T}\right) + \frac{H_m}{T_m} + B_1.(T - T_m) + B_0.\ln\left(\frac{T}{T_m}\right)$$

Equation 2.13

Applying the same logic and strategy, it is also possible to calculate the enthalpy changes ($\Delta H(T)_{c-sc}$) and free energy changes ($\Delta G(T)_{c-sc}$) between crystal and supercooled liquid with **Equation 2.14** and **Equation 2.15**, respectively.

$$\Delta H(T)_{c-sc} = \frac{C_1}{2}.\left({T_m}^2 - T^2\right) + C_0.(T_m - T) + H_m + \frac{B_1}{2}.\left(T^2 - {T_m}^2\right) + B_0.(T - T_m)$$

Equation 2.14

$$\Delta G(T)_{c-sc} = \Delta H(T)_{c-sc} - T\Delta S(T)_{c-sc}$$

Equation 2.15

If we are considering the excess of the free energy between the glass and crystal, for temperatures below glass transition the expressions for the variation in enthalpy ($\Delta H(T)_{c-g}$) and entropy ($\Delta S(T)_{c-g}$) are given by **Equation 2.16** and **Equation 2.17**, respectively.

$$\Delta H(T)_{c-g} = \frac{C_1}{2}.\left({T_m}^2 - T^2\right) + C_0.(T_m - T) + H_m + \frac{B_1}{2}.\left({T_g}^2 - {T_m}^2\right) + B_0\left(T_g - T_m\right) + \frac{D_1}{2}\left(T^2 - {T_g}^2\right) + \\ + D_0\left(T - T_g\right)$$

Equation 2.16

$$\Delta S(T)_{c-g} = C_1.(T_m - T) + C_{0.}\ln\left(\frac{T_m}{T}\right) + \frac{H_m}{T_m} + B_1.\left(T_g - T_m\right) + B_0.\ln\left(\frac{T_g}{T_m}\right) + D_1.\left(T - T_g\right) + D_0.\ln\left(\frac{T}{T_g}\right)$$

Equation 2.17

3

Results and Discussion

3.1 Characterization of APIs

As mentioned before, each API was characterized, in the DSC, using a program that consisted of heating the crystalline samples above melting (~190ºC), cooling rapidly below T_g to generate the amorphous material and heating up again above the glass transition temperature. All thermograms collected for the first heating ramp, in **Appendix A**, showed an endothermic peak typical of the melting of crystalline samples. For all APIs, during cooling no crystallization events were detected. In the second heating ramp, the glass transition was detected together with an enthalpy overshoot, which corresponds to the enthalpic relaxation recovery. The temperatures and thermal parameters associated to each event are represented in **Table 3.1**.

Table 3.1- Summarized thermal properties of each API and ASD

API	T_m (ºC)	ΔH_m (J.g^{-1})	T_g (ºC)	ΔH_{relax} (J/g)	$\Delta c_p(T_g)$ (J/g.ºC)
Indomethacin	158.8	103.69	45.9	2.370	0.368
Itraconazole	164.8	80.67	58.2	1.010	0.410
Nifedipine	170.7	104.88	46.4	1.960	0.349
Cimetidine	138.3	154.22	46.9	3.896	0.567
Sulindac	179.2	85.38	73.7	2.200	0.326
Warfarin	156.2	111.37	59.8	5.388	0.542
Physical mix A	175.2	75.45	58.7	1.176	0.350
Physical mix B	175.6	81.49	45.0	1.303	0.327
Physical mix C	174.9	53.88	42.8	1.311	0.291

In the case of the different nifedipine ASDs, the results showed that the normalized enthalpy of fusion is lower than that of the pure nifedipine. Since this enthalpy contains contributions from the enthalpy of melting and mixing, this result indicates that exothermic mixing occurred. In such cases, the interactions between the drug and the polymer are considered to be strong [44]. In all thermograms, the second heating ramp showed a single glass transition which suggests that complete mixing was achieved.

An interesting case of drugs that exhibit similar T_g but different crystallization behaviors during heating is that of nifedipine and indomethacin. As shown in **Figure 3.1**, while nifedipine crystallizes above T_g, around 90ºC, indomethacin remains in the supercooled liquid state, thus suggesting that molecular mobility and T_g are not the only factors influencing the tendency for crystallization. It can be concluded that glass transition temperature is not an indicator of stability. It is even possible to see that, during heating, nifedipine crystallizes around 90ºC and converts to the initial polymorph around 110ºC (same T_m as the starting polymorph). This behavior was found in the literature and corresponds to the crystallization of form B followed by conversion into form A, the most stable form [59].

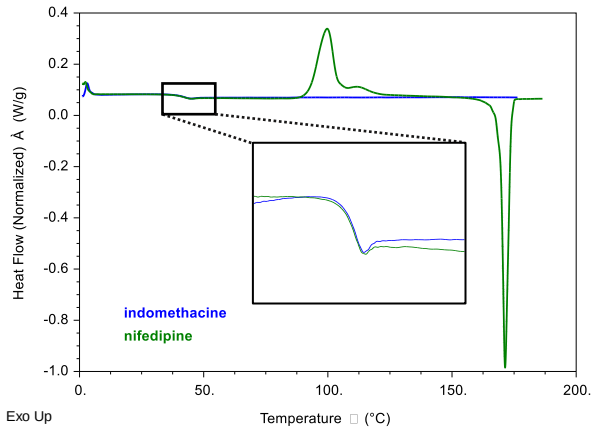

Figure 3.1- Indomethacin and nifedipine behaviour during heating

Regarding the analysis of APIs with DRS, some differences in the thermal properties were found by comparison with the DSC results. **Table 3.2**. shows that the T_g of nifedipine, indomethacin and sulindac determined with DRS are slightly lower, compared to those obtained with the DSC (**Table 3.1**) These differences can be explained by the application of different cooling rates for amorphization, using the two techniques. Regarding the changes in molecular mobility observed, two types of relaxations were identified: ones that are more intense at higher frequencies, α-relaxations, and the others that are more visible at lower frequencies, sub α- relaxations. Looking at the dielectric loss graphs in **Figure 3.2** to **Figure 3.4**, it is evident that there is a shift in the peak temperatures as a function of frequency. Regarding the relaxation maps in **Figure 3.2** to **Figure 3.4**, it is possible to see that the sub-α relaxations follow an Arrhenius behavior (linear change with the inverse temperature) and exhibit a lower activation energy, taken as the slope of these plots. With respect to the α- relaxation process, the change in relaxation time with temperature is usually described by the VTF model. DRS data were fitted to this model to determine the glass transition temperature, assuming that at T_g the relaxation time is equal to 100s, which is thought to be reasonable. Nevertheless, the T_g results were slightly different from those determined with the DSC. As seen before, in the DSC, the DRS results for nifedipine showed the same tendency for crystallization during heating.

However, it must be pointed out that **Figure 3.3**, only shows a discontinuity near 90ºC, corresponding to the crystallization into the metastable polymorph.

Table 3.2- Determination of T_g by DRS measurements

API	T_g(ºC)
Indomethacin	41
Nifedipine	41
Sulindac	57

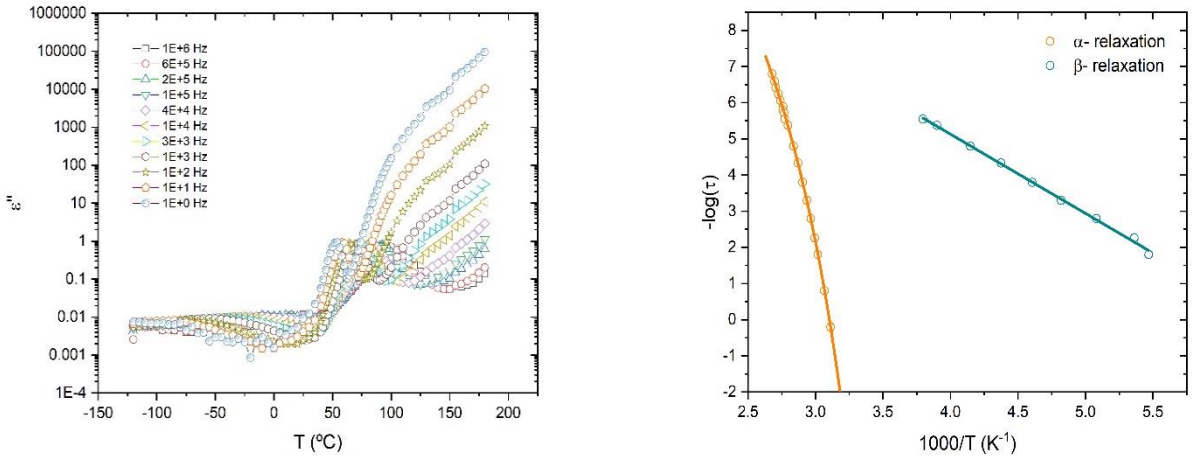

Figure 3.2- Dielectric loss vs Temperature (left) and relaxation map (right) of indomethacin

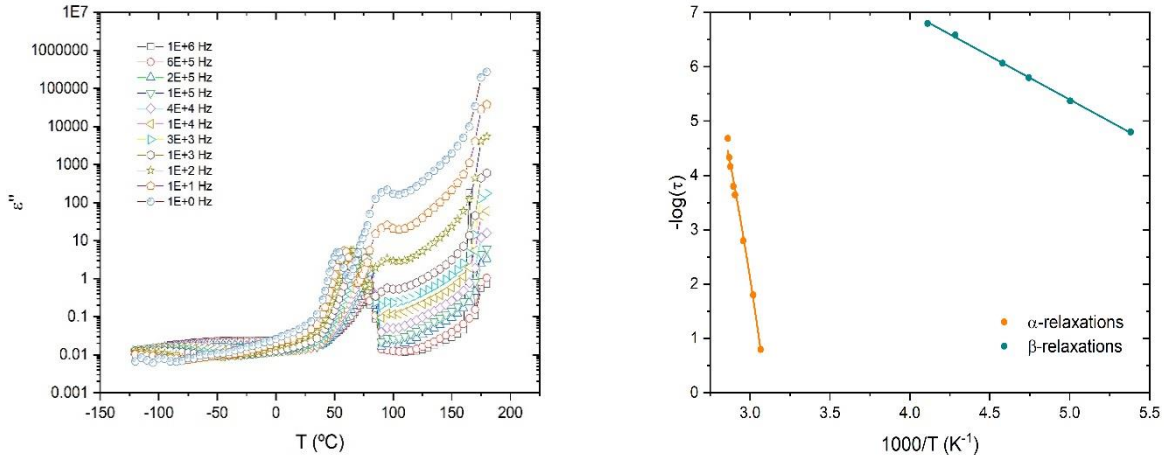

Figure 3.3- Dielectric loss vs Temperature (left) and relaxation map (right) of nifedipine

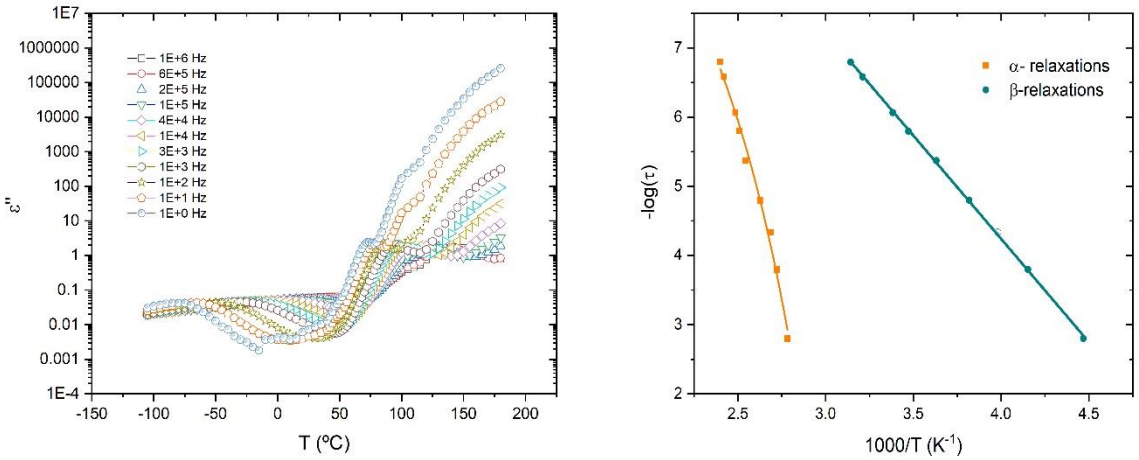

Figure 3.4- Dielectric loss vs temperature (left) and relaxation map of sulindac

The fitting parameters obtained with **Equation 2.1** and **Equation 2.5**, for the different relaxation processes can be found in **Table 3.3**. In terms of apparent activation energy, the three APIs seem to possess similar values, therefore indicating that around T_g the molecular mobility is similar. However, when looking at the activation energies of the sub α- relaxations, it is possible to see that sub α -relaxation of nifedipine requires a lower activation energy, when compared to the other APIs. As this type of motions are believed to be the precursors of α-relaxations [60], the fact that nifedipine exhibits a smaller activation energy, compared to indomethacin, can explain the different behaviors during heating.

Table 3.3- Fitting parameters of non-linear and linear relaxation functions

	VTF fitting				**Arrhenius fitting**
API	τ_0(s)	B	T_0(K)	$E_a(T_g)$ (kJ/mol)	E_a (kJ/mol)
Indomethacin	2.37×10^{-17}	2848.5	248	530	41.9
Nifedipine	1.00×10^{-18}	3429.1	240	507	30.7
Sulindac	4.74×10^{-13}	1849.6	274	533	57.2

With respect to the Kauzmann temperatures, determined when the difference in entropy between the supercooled liquid and the crystal is zero, values are presented in **Table 3.4**. Amorphous itraconazole is expected to be the most stable drug, at room temperature, since it is the only drug that shows a T_k higher than 298.15 K. As a result, itraconazole is considered a good candidate for amorphization. Regarding the

Kauzmann temperature of the ASDs, the values obtained were higher than those of pure nifedipine (267.7 K), which strengthens the idea that polymer stabilization in the ASD lowers the molecular mobility. The determination of this temperature can be a good indicator of the recommended storage temperature since the mobility of the amorphous material is lower at this temperature.

Table 3.4- Summary of the Kauzmann temperatures determined for each API (n=3) and ASD (n=1)

API	T_k(K)
Indomethacin	277.4 (±11.5)
Cimetidine	251.5 (±0.7)
Sulindac	188.9 (±27.0)
Itraconazole	303.3 (± 8.1)
Warfarin	254.0 (±1.4)
Nifedipine	267.7 (±3.1)
Physical mix. A	294.0
Physical mix. B	285.0
Physical mix. C	271.0

3.2 Evaluation of glass relaxation

3.2.1 Impact of different cooling rates on relaxation

These experiments revealed that applying a faster cooling rate leads to an increase in T_g, as shown in **Figure 3.5** to **Figure 3.13**. This effect demonstrates that the glass transition is a kinetic phenomenon. However, for itraconazole, the glass transition temperatures measured during the heating ramp followed the opposite trend. This effect may be explained by the presence of two liquid crystal transitions immediately above T_g that eliminate the thermal history of the supercooled liquid generated by different cooling rates. As a result, the effect of cooling rate is limited to a short temperature range below T_g, where molecular mobility and relaxation kinetics are significantly reduced. In addition to changes in T_g, the enthalpic recovery at T_g increased for slower cooling rates, which is explained by the fact that a slower cooling rate allows more time for relaxation to occur, as it falls out of the equilibrium. This increased relaxation results in a greater enthalpic gain at T_g.

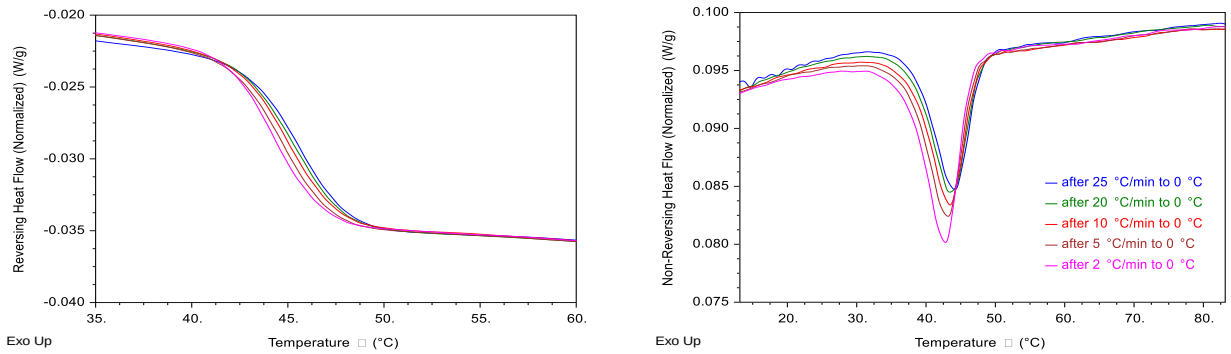

Figure 3.5- Impact of different cooling rates: Indomethacin

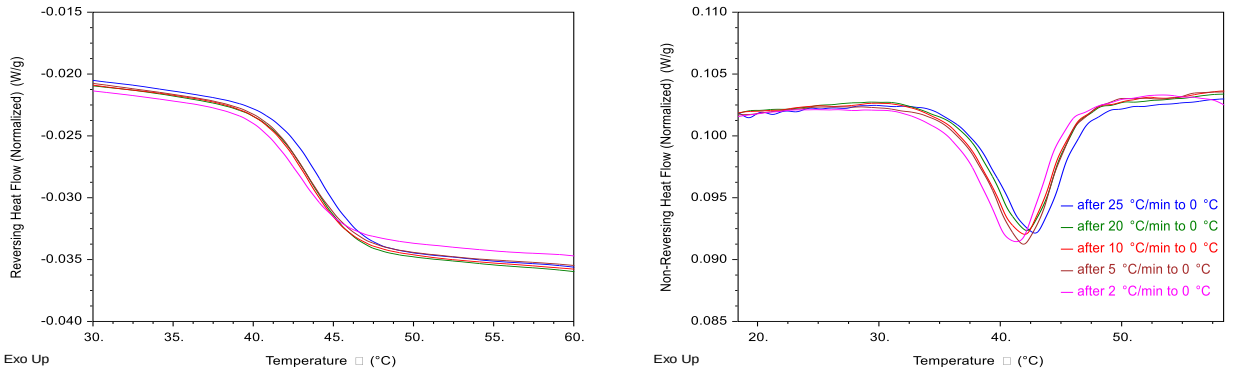

Figure 3.6- Impact of different cooling rates: Nifedipine

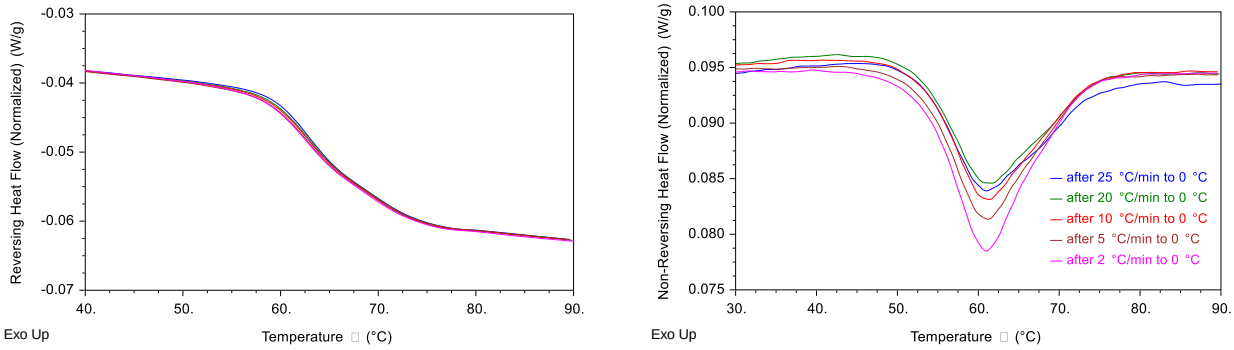

Figure 3.7- Impact of different cooling rates: warfarin

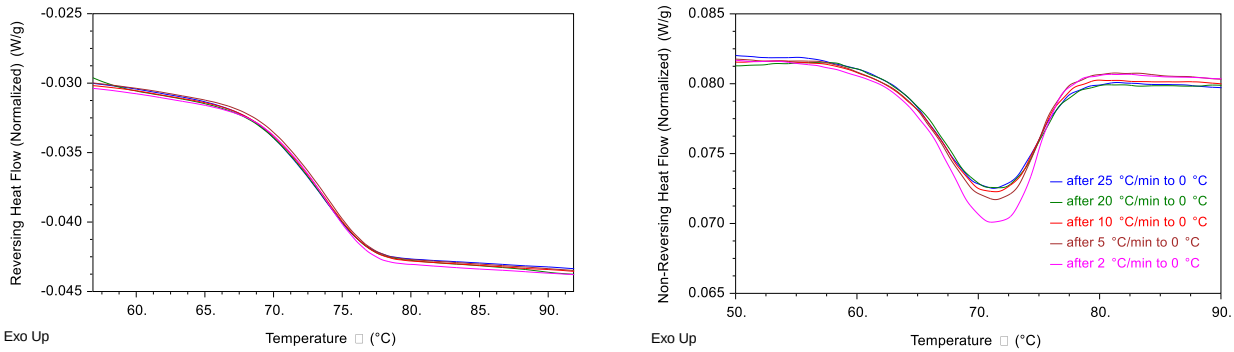

Figure 3.8- Impact of different cooling rates: Sulindac

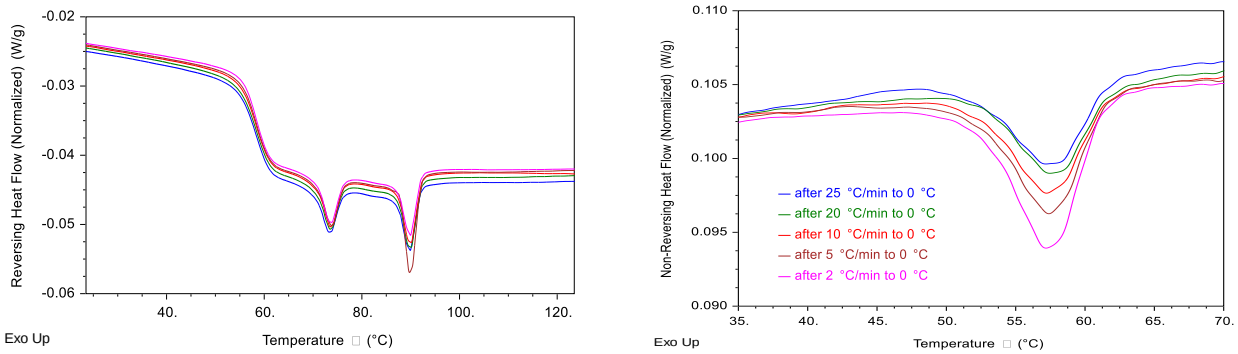

Figure 3.9- Impact of different cooling rates: Itraconazole

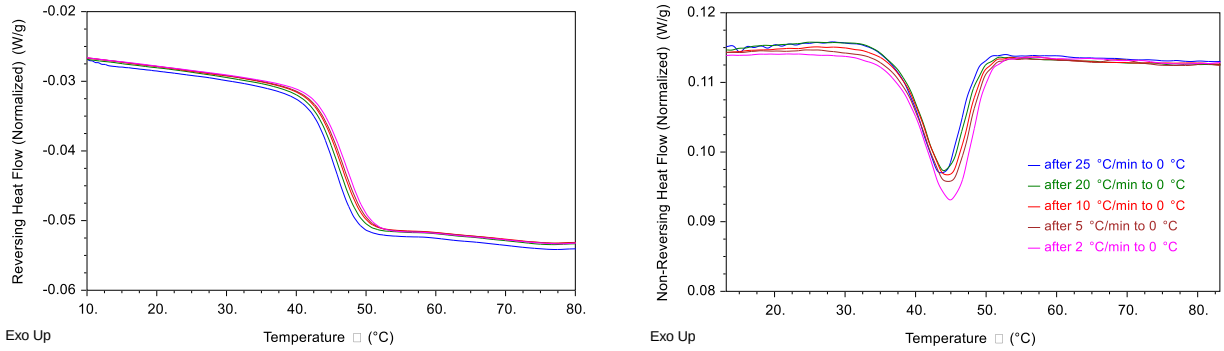

Figure 3.10- Impact of different cooling rates: cimetidine

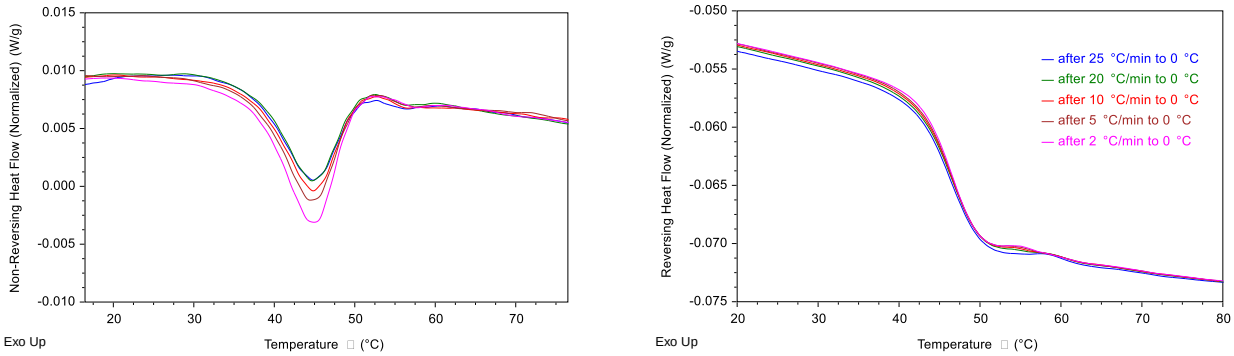

Figure 3.11- Impact of different cooling rates: physical mix. B

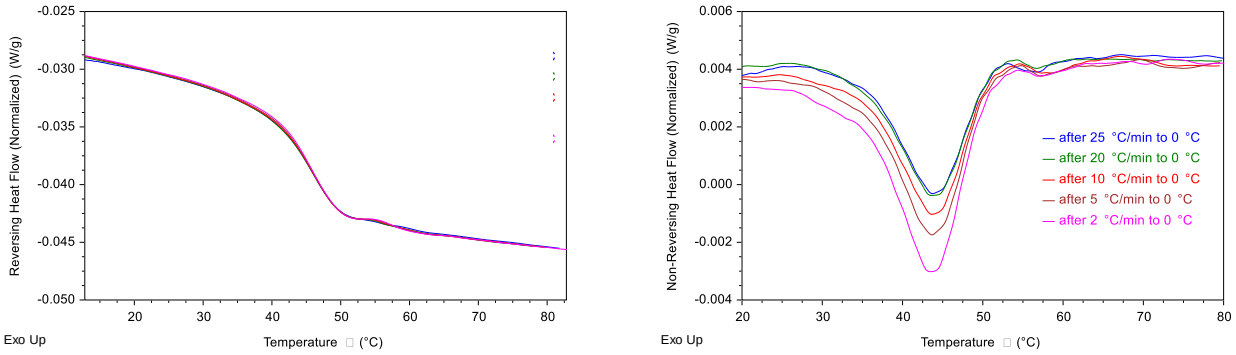

Figure 3.12- Impact of different cooling rates: physical mix. C

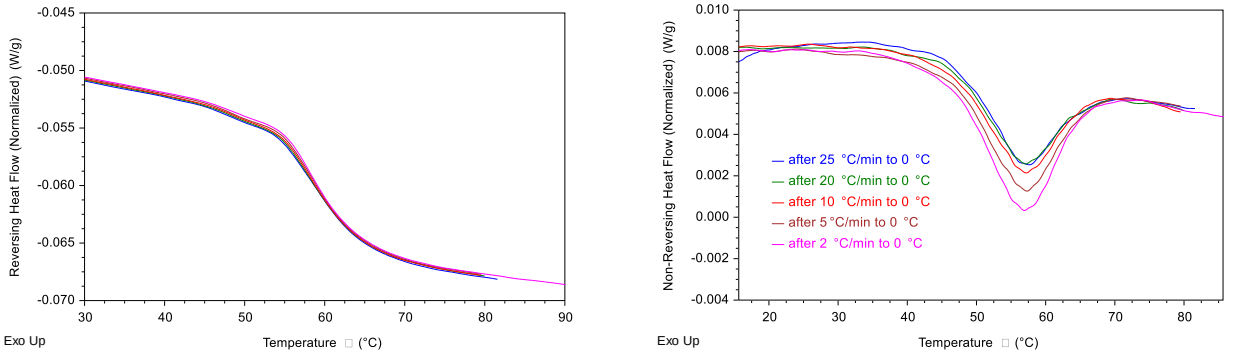

Figure 3.13- Impact of different cooling rates: Physical mix. A

3.2.2 Determination of the kinetic fragility

With the results obtained in the previous section, it was also possible to assess the molecular mobility drugs by estimating the fragility index (m) by the **Equation 1.21** and **Equation 2.9**. **Table 3.5** presents the values of m determined with the different techniques, DRS and DSC. Despite the different values obtained with the two methods, which are intrinsic to the type of method, it is evident that all APIs can be classified as fragile. Therefore, the structural configuration of materials, around T_g, is more sensible to small variations in temperature. The differences between the values can be related to the application of different cooling rates but also because of, in the case of DRS measurements, the assumption that at T_g, the relaxation time is 100 s. Besides this, in this technique, the fragility index is determined with fitting parameters that may reproduce some errors too.

Table 3.5- Values of fragility measured by DSC and DRS

API	Fragility by DSC	Fragility by DRS	Literature
Indomethacin	107	88	83 [61]
Sulindac	179	84	-
Nifedipine	180	84	84 [62]
Itraconazole	222	-	-
Warfarin	69	-	-
Cimetidine	239	-	-
Physical mix.A	240	-	-
Physical mix B	180	-	-
Physical mix C	203	-	-

3.2.3 Relaxation below T_g

The purpose of this study was to evaluate the molecular mobility by monitoring the extent of relaxation during the annealing experiments in the DSC. For all APIs, the enthalpy recovery at T_g increased with the annealing time, as it can be seen from **Figure 3.14** to **Figure 3.16**. Regarding the maximum enthalpy recovery values obtained after 12 hours, no clear correlation was found between annealing temperature and this maximum value. For indomethacin and itraconazole, the maximum enthalpy recovery, after 12h, was higher for the highest temperature. For all others, the opposite was observed. These results were not unexpected since the enthalpy gain at a certain annealing time depends on two factors that show opposite effects as a function of temperature: the kinetics of relaxation that are higher at higher temperatures and the enthalpy difference between the glass and the supercooled liquid which is lower for higher temperatures. The differences observed for the different annealing temperature were not significant since the experiments were conducted at temperatures that only differed in 5ºC.

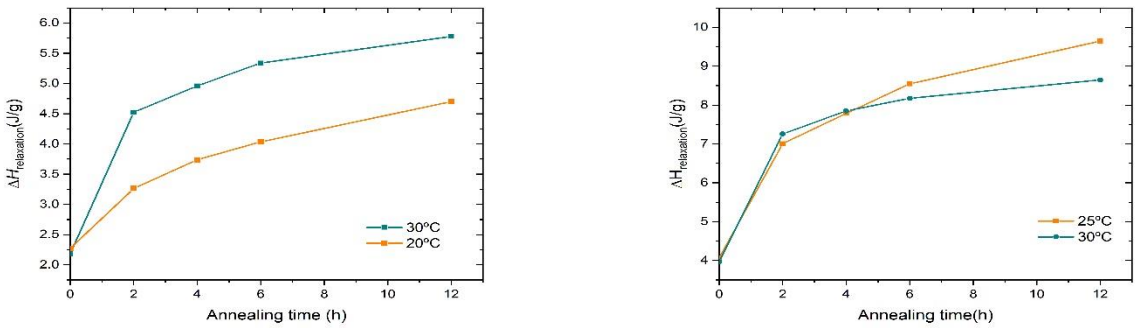

Figure 3.14-- Enthalpy of relaxation vs annealing time of indomethacin (left) and cimetidine (right)

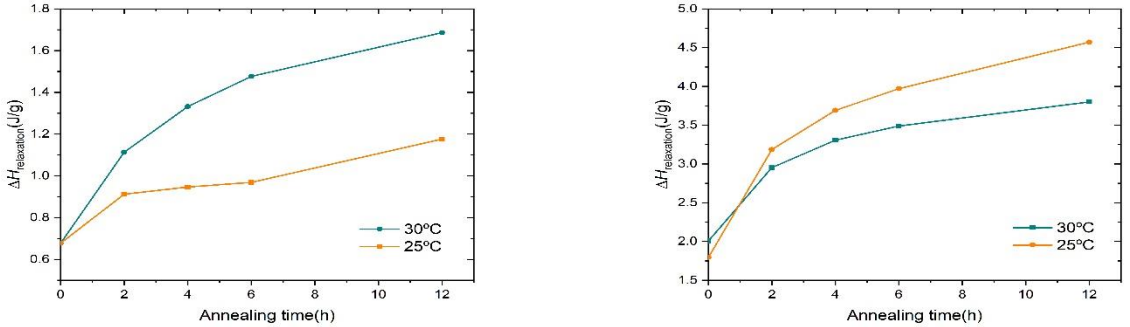

Figure 3.15- Enthalpy of relaxation vs annealing time: Itraconazole (left) and nifedipine (right)

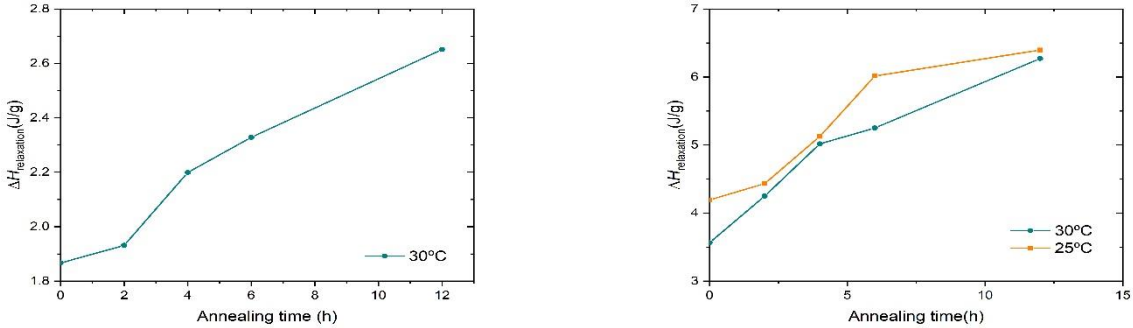

Figure 3.16- Enthalpy of relaxation vs annealing time of sulindac (left) and warfarin (right)

Regarding the results obtained for the different ASDs of nifedipine, the variations in enthalpy of relaxation with time depend not only on the type of polymer, but also on the drug load. In **Figure 3.17**, it is possible to see that the mixture that contains PVP K29/32 (Phys. Mixture A) has lower enthalpies of relaxation, when compared to the mixtures with Eudragit EPO and pure amorphous nifedipine. In the case of the mixtures with the same polymer but different drug loads, although the magnitude of the values is different, the variations with time are similar. Correlations with stability are difficult to do, with these results alone, since the enthalpy of relaxation at a certain time depends on two factors: kinetics of relaxation and the thermodynamic maximum for relaxation.

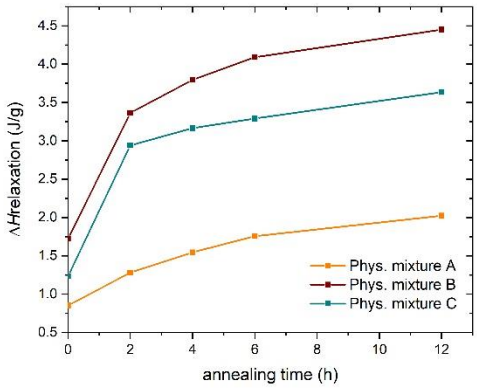

Figure 3.17- Variation of the enthalpy of relaxation of the ASDs with time

Regarding the estimations of the maximum enthalpy of relaxation allowed (ΔH_∞) at 30ºC, the method found in the literature (**Equation 1.14**) and the one used in this project (**Equation 2.14** and **Equation 2.16**) present a significant difference (**Table 3.6**). Estimations with the method found in the literature [47] yielded unreliable results, as shown in the case of indomethacin. Considering the maximum enthalpy of relaxation determined with that method, 5.87 J/g, at the end of the 12 hours of annealing, the samples would be completely relaxed, according to **Figure 3.14**, which is not true. The literature method presents some limitations as it considers that the heat capacity difference between glass and supercooled liquid is independent of temperature and equal to Δc_p (T_g). On the other hand, the estimation of ΔH_∞ as the enthalpy difference between the glass and the supercooled liquid gives more realistic results but it also contains some small errors since the heat capacity does not vary linearly with temperature.

Table 3.6- Estimation of the maximum enthalpy of relaxation at 30ºC :APIs (n=3) and ASD (n=1)

API	ΔH_{∞}(J/g) literature method	$\Delta H_{sc\text{-}g}$ (J/g)
Cimetidine	9.60	12.74 (±1.83)
Indomethacin	5.87	9.11(±0.26)
Itraconazole	11.57	13.62(±1.45)
Warfarin	16.17	15.84(±2.45)
Sulindac	14.24	13.17(±0.32)
Nifedipine	5.71	5.80(±0.12)
Physical mix. A	10.04	9.55
Physical mix. B	4.92	10.40
Physical mix. C	3.73	9.07

3.3 Accelerated stability study

A preliminary stability study was conducted under accelerated conditions (120ºC) to evaluate the crystallization tendency of the different drugs, at high temperatures. Experiments were conducted in the DSC and samples were held for 12 hours, at an elevated temperature closed to the melting. As it can be seen in **Figure 3.18**, during the 12 hours only indomethacin and Itraconazole crystallized, but at different times, 286 min and 63 min, respectively. Crystallization was detected as an increase in heat flow (figure on the left) and by the presence of an endothermic peak after heating above melting (figure on the right). Furthermore, it is possible to see that indomethacin crystallized into a different polymorph, which according to the literature corresponds to the γ form [63]. Although thermodynamically the occurrence of crystallization is more favorable at lower temperatures, the increase in temperature also increases the molecular mobility and, consequently, the kinetics of crystallization induce nucleation. Contrary to the results obtained in the typical amorphization experiments in the DSC,**Figure 3.1**, nifedipine did not crystallize at this temperature. This difference can be explained by different paths taken to reach the same target temperature and the occurrence of different transitions along those paths. For example, in the typical amorphization experiments, crystallization into form A occurs from polymorph B, which may be more thermodynamically favorable than direct crystallization from the liquid, at high temperatures.

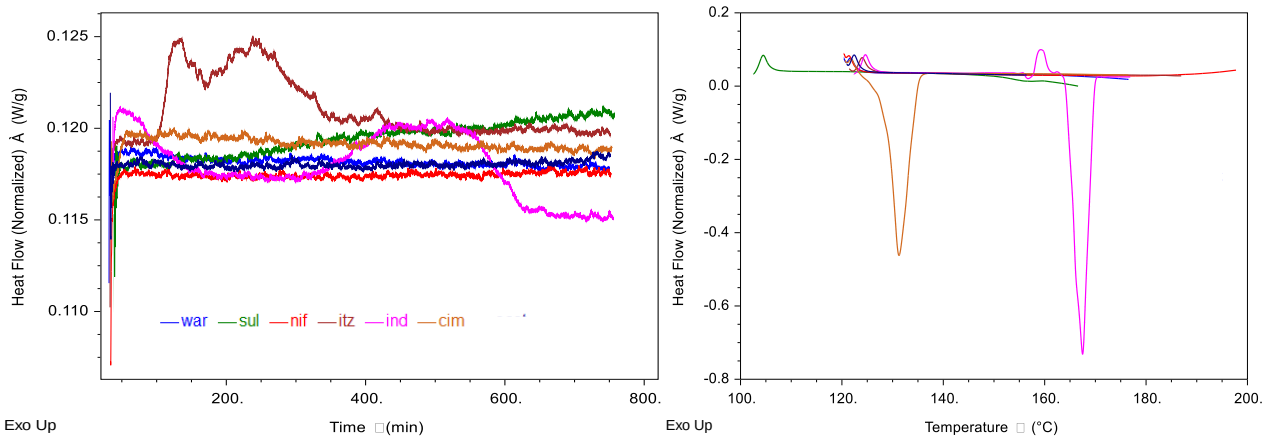

Figure 3.18- Stability at 120ºC

3.4 Long-term stability study

To facilitate the discussion of the results obtained during the stability study, conducted at 30ºC, the results for each drug will be evaluated separately.

3.4.1 Indomethacin

The DSC results obtained during stability showed that the materials generated by melt-quenching, in the hot plate, were different from those prepared inside the DSC, during the amorphization experiments. The thermograms obtained at all time points show that the drug crystallizes during heating, contrary to amorphous samples prepared in the DSC. These results indicate that the preparation technique and procedure have impact on the thermal history and physical stability of amorphous indomethacin. As it can be seen in **Figure 3.19**, during the stability, all thermograms showed two exothermic peaks corresponding to the crystallization event followed by a polymorphic conversion, and also other two endothermic events that correspond to the respective melting points. According to the values found in literature, the polymorphs correspond to β and ɣ with melting onset temperatures of 148 ºC and 160ºC [63].

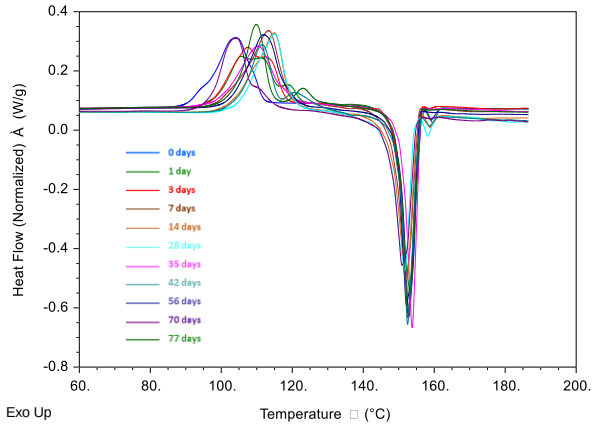

Figure 3.19- Thermograms obtained during stability: indomethacin by DSC

It was also observed a decrease in the T_g (**Figure 3.20**, right) which is inherent to the variability during the preparation of the samples. Although it was difficult to determine the onset of crystallization, by DSC, a decrease in the enthalpy of relaxation was detected, after 4 weeks, suggesting that crystallization occurred at this time (**Figure 3.20**, left).

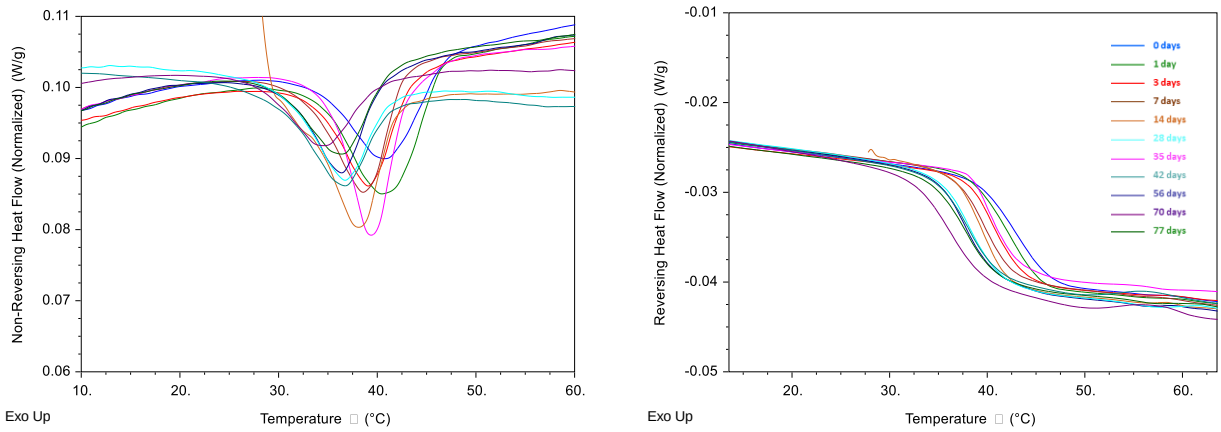

Figure 3.20- Evolution of enthalpy of relaxation (left) and T_g (right) for indomethacin by DSC

On the other hand, XRPD results showed that indomethacin samples start to crystallize after 42 days, **Figure 3.21**. However, a previous visual inspection after 32 days showed the presence of crystals. The lack of agreement between the results obtained for onset of crystallization, determined with the two techniques, is attributed to differences in the preparation of samples. The XRPD results also showed that samples crystallized to the initial form, the most stable, during stability. It must be pointed out, that even through the onset was detected after 42 days, visual inspection of the remaining samples in the oven showed that not all of them had crystallized.

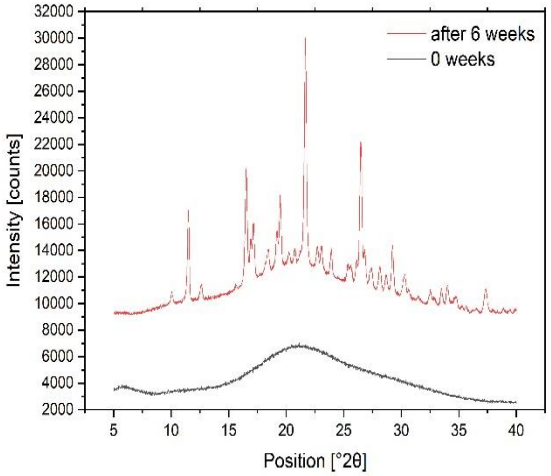

Figure 3.21- Diffractograms obtained during the stability study: indomethacin (XRPD)

3.4.2 Nifedipine

During the stability study, nifedipine was the first drug to crystallize. Once again, the onset of crystallization determined with the two techniques did not match due to differences in the preparation of samples. The DSC thermograms, in **Figure 3.22**, show the presence of small endotherms of melting since the day that the samples were prepared, which confirms the presence of crystals in the samples. During the stability study, nifedipine crystallizes to a polymorph that is different from the most stable form (different melting temperatures). This observation was also demonstrated by the XRPD results, **Figure 3.24**. In this case, however, samples just showed signs of crystallization after 3 days. The peak detected at 38 º2θ is relative to the aluminum foil used to prepare the initial samples. The diffractogram of the initial crystalline form is presented in **Appendix B**.

.

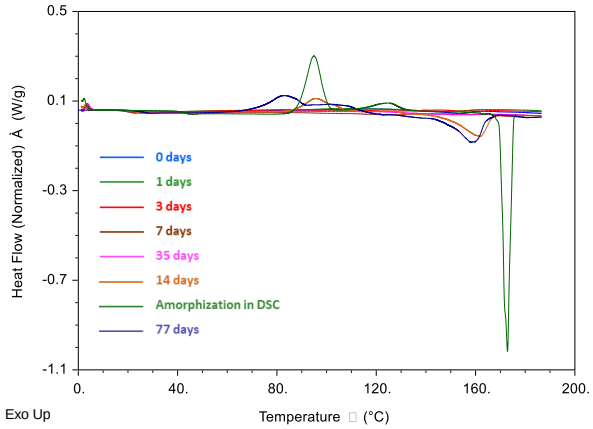

Figure 3.22- Total heat flow: nifedipine (DSC)

Regarding the results represented in **Figure 3.23**, it is possible to observe the impact of the variability of the preparation of the amorphous forms on T_g. With respect to the enthalpy of relaxation, this parameter increased during the days.

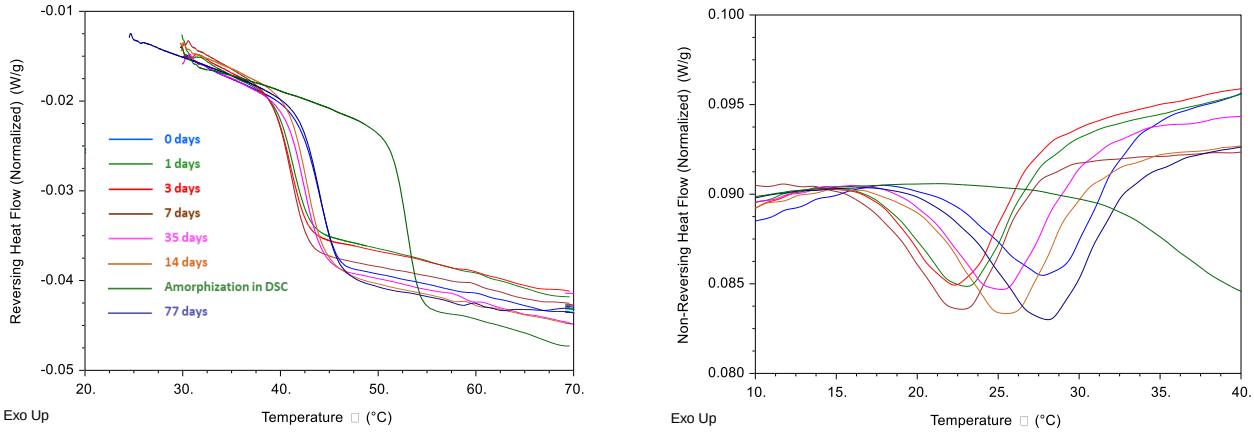

Figure 3.23- Evaluation of T_g (left) and enthalpy of relaxation (right) for nifedipine by DSC

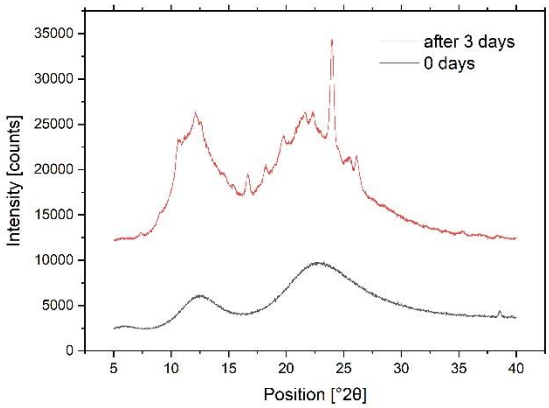

Figure 3.24- Detection of the onset of crystallization by XRPD: nifedipine

Additionally, another stability study was conducted at 5ºC to see how the molecular mobility changes with temperature, and consequently, how this variation affects the recrystallization behavior. In **Figure 3.25** it is possible to see that the onset of crystallization is not significantly different from that determined by XRPD, at 30ºC. Small diffraction peaks were also observed after 3 days. However, the intensity of those peaks increases much faster at 30ºC, therefore showing that temperature has more impact on crystal growth than nucleation.

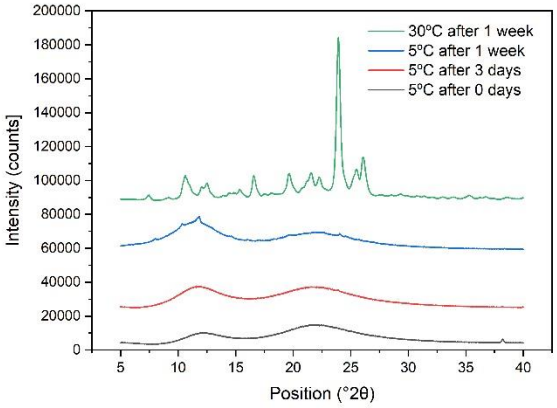

Figure 3.25- Detection of the onset of crystallization for nifedipine at 30ºC and 5ºC by XRPD

3.4.3 Cimetidine

According to the diffractograms presented in **Figure 3.26**, samples start to crystallize after 59 days. However, the onset of crystallization detected in the DSC is not in agreement. In **Figure 3.27** it is possible to observe melting peaks at temperatures close to T_m of cimetidine, after 1 week.

It must be pointed out that although crystallinity was detected by XRPD in the 59 days sample, in the visual inspection during the rest of the stability study, none of the remaining samples showed any signs of crystallinity. Therefore, this means that the onset detected may not be representative.

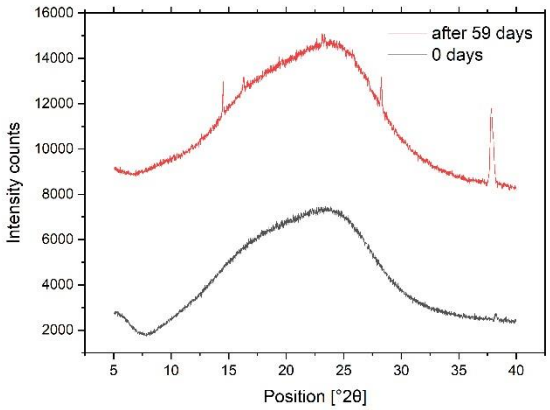

Figure 3.26- Detection of the onset of crystallization: cimetidine by XRPD

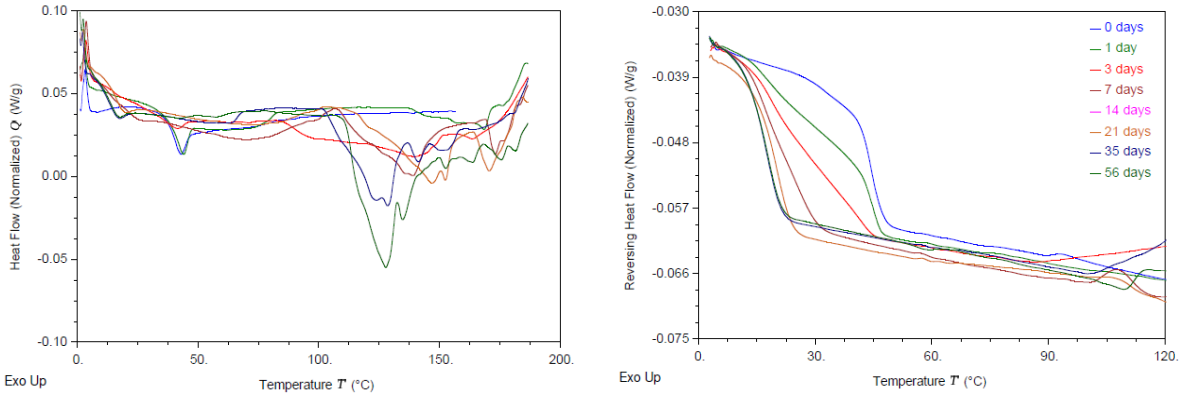

Figure 3.27- Evolution of the enthalpy of relaxation (left) and Tg (right) for cimetidine by DSC

A different sample of cimetidine was prepared by solvent evaporation and analyzed immediately by the two techniques. In **Figure 3.28**, it is possible to see that both techniques confirm the presence of crystals, therefore demonstrating that the preparation technique has impact on the physical stability of the amorphous drugs.

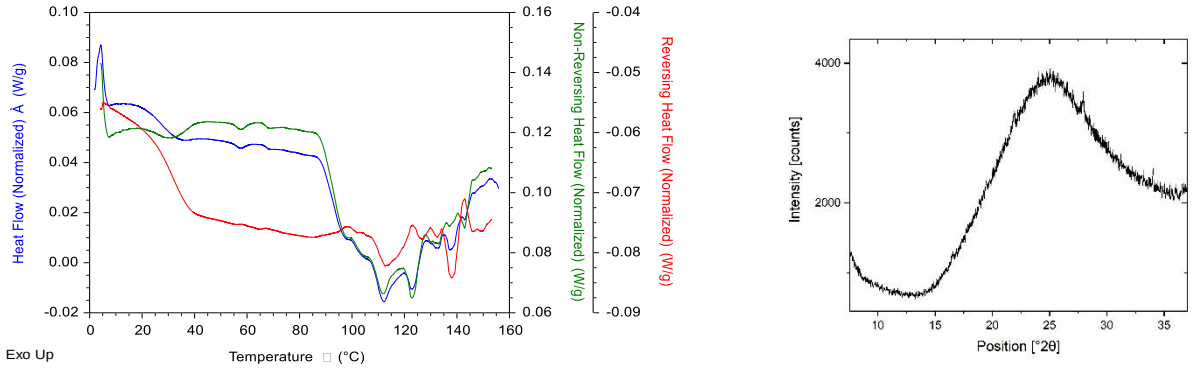

Figure 3.28- Detection of crystallinity in amorphous cimetidine prepared by solvent evaporation by DSC (left) and XRPD(right)

3.4.4 Itraconazole

The XRPD results show that this drug remained in the amorphous form during the whole stability study (**Figure 3.29**). The fact that the stability temperature is near the estimated T_k (303.3 K) explains this behavior. That is because at this temperature the amorphous form has very low mobility. Once again, the peak detected around 38 º2θ corresponds to the aluminum foil used to prepare the samples in the hot plate.

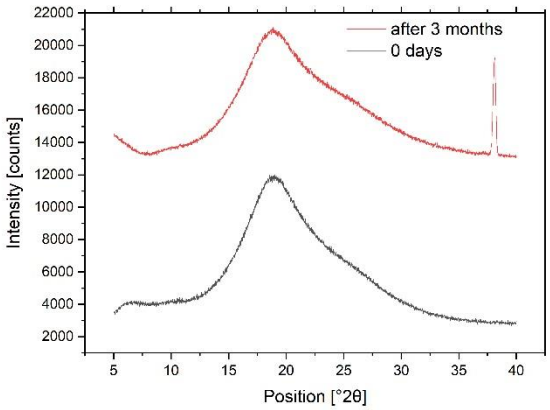

Figure 3.29- Detection of the onset of crystallization: itraconazole by XRPD

The DSC results (**Figure 3.30**) showed that the stability samples prepared by melt-quenching exhibit different molecular mobility in comparison to the ones prepared in *situ* in the DSC. Such differences indicate that the preparation technique has impact on the physical stability. With respect to the relaxation phenomenon, **Figure 3.31**, a clear increase in the enthalpic recovery was observed, with time, consistent with the loss of excess energy typical of the relaxation process.

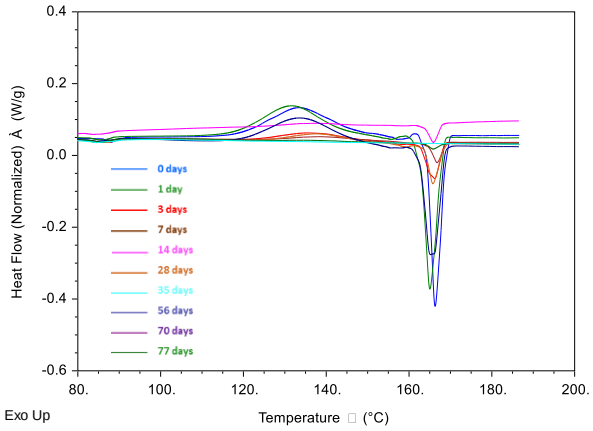

Figure 3.30- Evolution of the total heat flow: itraconazole by DSC

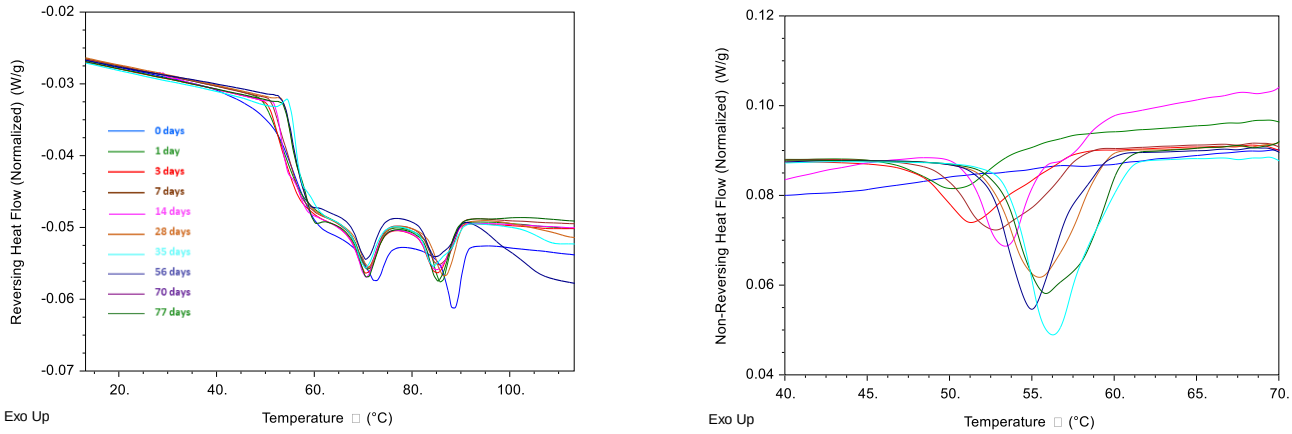

Figure 3.31- Evolution of T_g (left) and enthalpy of relaxation (right) for itraconazole by DSC.

3.4.5 Sulindac

The diffractograms in **Figure 3.32** show that this drug was stable during the whole stability study. An identical result was obtained in the DSC. However, contrary to the other APIs, an increase in T_g was observed with stability time and also in comparison to the T_g determined by amorphization, in situ, in the DSC. This increase in T_g is explained by variability associated with the sample preparation technique, as demonstrated by **Figure 3.33**. The application of different cooling rates to the molten drug, prepared in the hot plate, has an impact on T_g since the excess energy entrapped in the glass depends on the cooling rate. Since this rate was difficult to control during preparation of the amorphous drugs, the DSC results reflect the variability inherent to sample preparation.

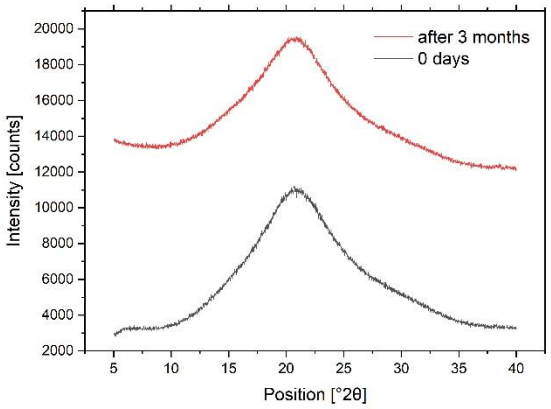

Figure 3.32- Detection of the onset of crystallization: sulindac by XRPD

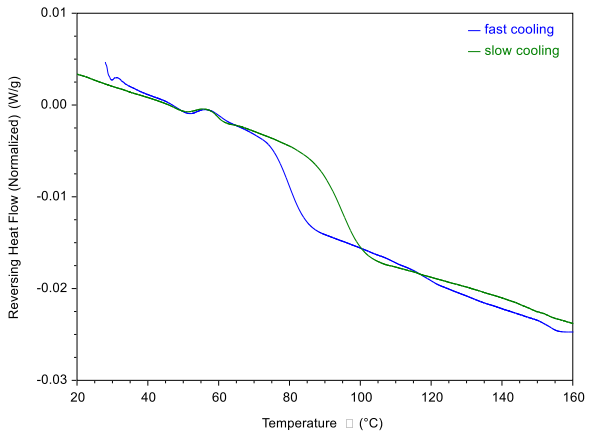

Figure 3.33- Impact of different cooling rates, applied during melt-quenching on T_g by DSC.

When looking at the variations in the relaxation enthalpy with time, **Figure 3.34**, it is clear that the enthalpy of relaxation is almost absent at all time points. This slowdown in physical ageing can explain the stability of this drug. However, the last samples already show some extent of relaxation.

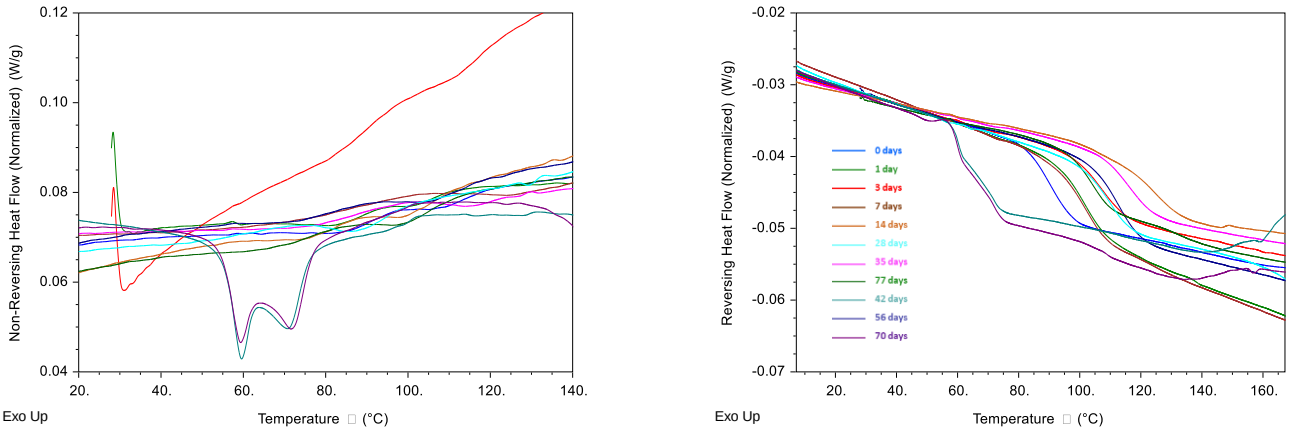

Figure 3.34- Evolution of enthalpy of relaxation (left) and T_g (right) for sulindac by DSC.

3.4.6 Warfarin

The diffractograms in **Figure 3.35**, show that this drug starts to crystallize after 42 days. On the other hand, the DSC thermograms do not allow determining the onset of crystallization since this API starts to degrade at temperatures above 120ºC. When looking at the relaxation endotherms (**Figure 3.36**), it is possible to see that the samples are getting closer to equilibrium since there is an increase in the enthalpy gain, with time.

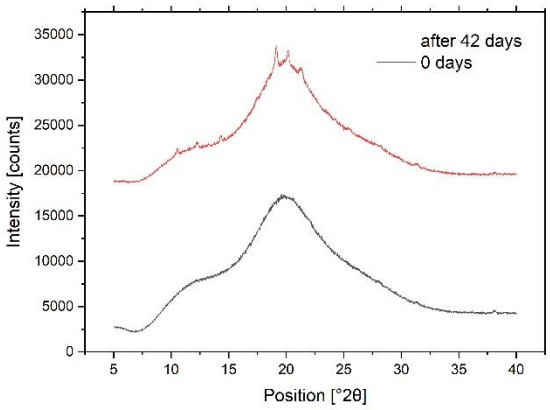

Figure 3.35- Detection of the onset of crystallization: warfarin by XRPD.

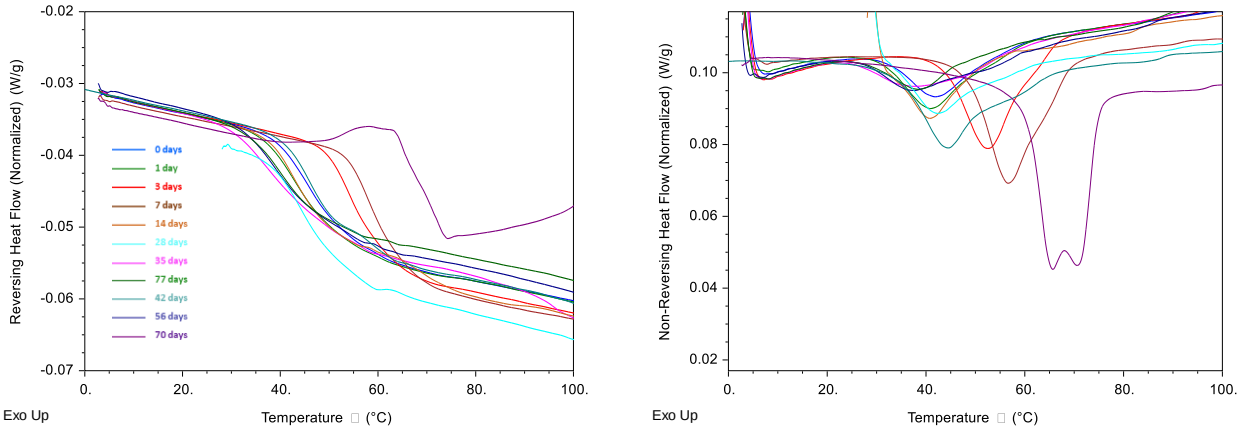

Figure 3.36- Evolution of T_g (left) and enthalpy of relaxation (right) for warfarin by DSC.

3.4.7 Amorphous solids dispersions

The XRPD results show very consistent results for all ASDs, since none of the samples crystallized in the 3-months period. Thus, the crystallization inhibition effect of the polymers is very clear, even in cases where the drug load is 80% w/w. The peak detected around 38 º2θ corresponds to the aluminum foil used to prepare the samples in the hot plate.

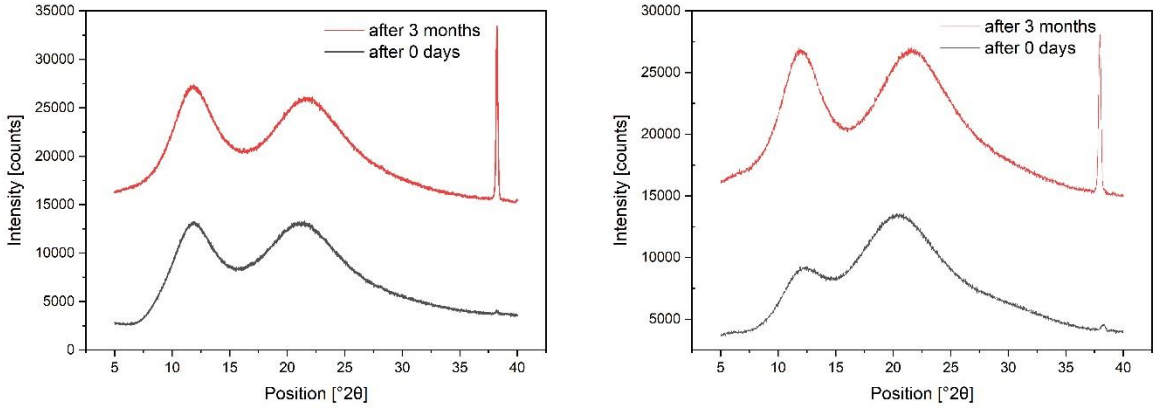

Figure 3.37- Detection of the onset of crystallization: Physical mix A (left) and C (right) by XRPD.

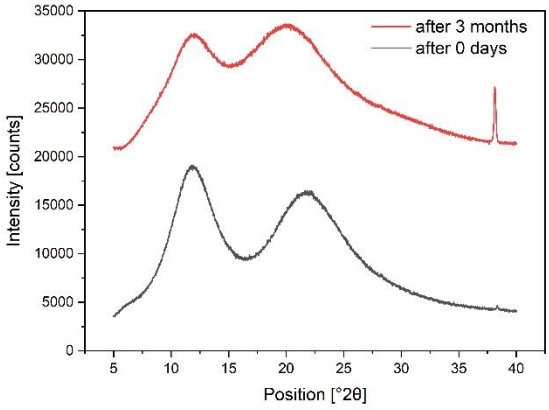

Figure 3.38- Detection of the onset of crystallization: Physical mix B by XRPD.

On the other hand, the DSC results show that, the crystallization inhibitory effect of polymers is not sufficient to avoid crystallization of nifedipine above T_g. Although no significant changes in T_g are observed over time, the values are lower compared to those obtained by melt-quenching in the DSC. This difference is explained by differences in the preparation technique used. Regarding the enthalpy of relaxation values, it is possible to observe that the mixtures with Eudragit EPO behave differently: for higher drug loads, the enthalpy gain at T_g is higher. For PVP K29/32 solid dispersions, the changes in relaxation enthalpy with time are not so significant, therefore suggesting that this polymer has a greater stabilization effect.

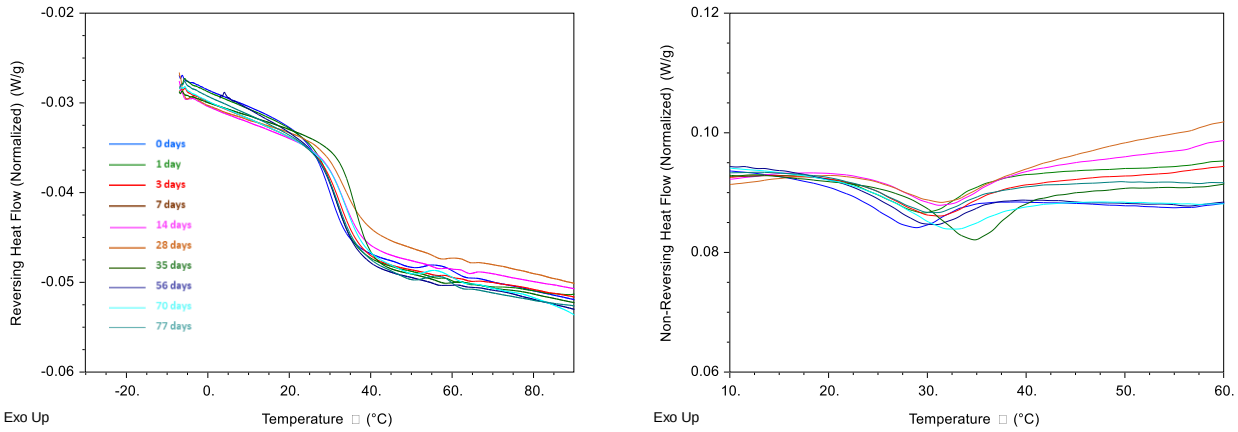

Figure 3.40- Evolution of T_g (left) and enthalpy of relaxation (right): Physical mix C by DSC.

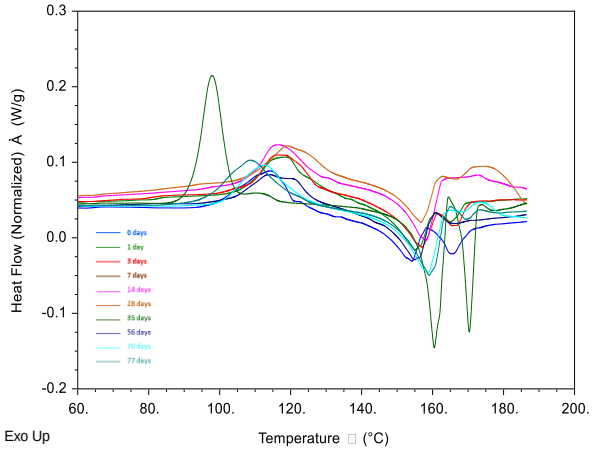

Figure 3.39- Total heat flow: physical mix C by DSC

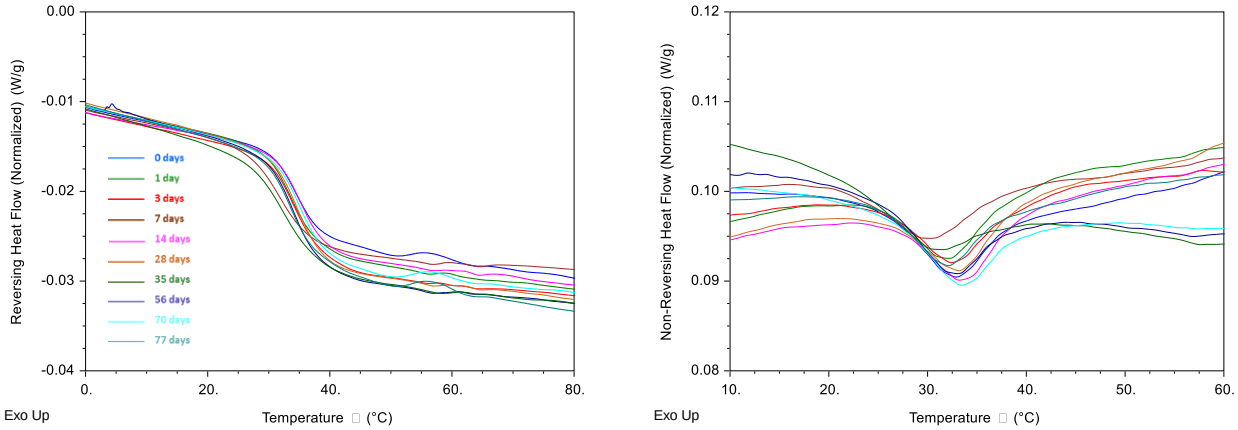

Figure 3.41- Evolution of T_g (left) and enthalpy of relaxation (right) for physical mix.B by DSC.

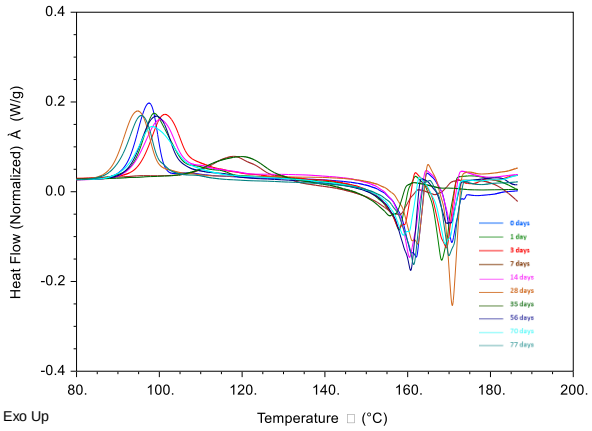

Figure 3.42- Total Heat flow: physical mix. B by DSC.

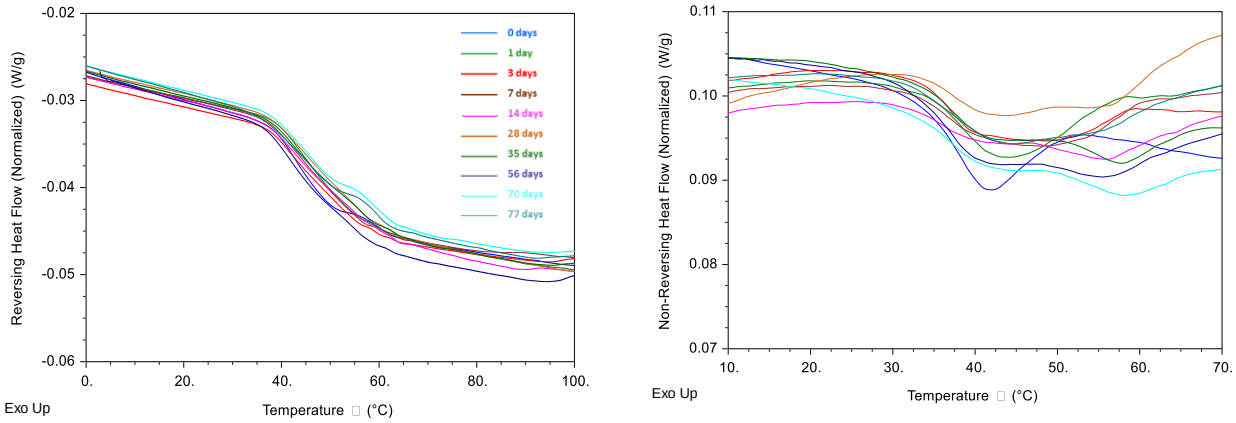

Figure 3.43- Evolution of T_g (left) and enthalpy of relaxation (right) for pysical mix.A by DSC.

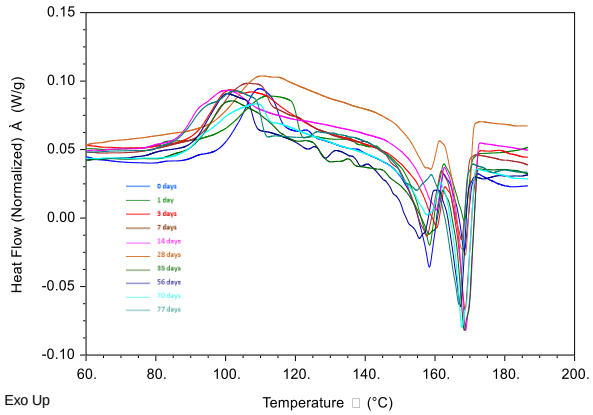

Figure 3.44- Total Heat flow for physical mix. A by DSC

3.5 Correlations

In order to gain a deeper understanding of which parameters may have impact on the physical stability of amorphous drugs, various correlations with the onset of crystallization, determined in the long-term stability study, are presented in this subchapter.

3.5.1 Correlation between the onset of crystallization and T_m

Since the melting temperature is characteristic of each API, it was decided to evaluate the possibility that this property correlates well with the onset of crystallization determined in the stability study. It must be pointed out that, in the case of ASDs, the offset of the dissolution endotherm was taken as T_m. According to **Figure 3.45**, there is no correlation between T_m and the onset of crystallization.

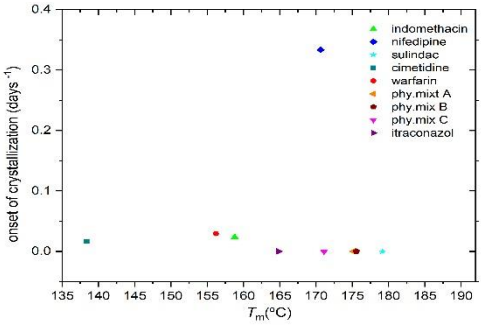

Figure 3.45- Correlation between the onset of crystallization and T_m

3.5.2 Correlation between the onset of crystallization and T_g

Another hypothesis tested was the correlation between the onset of crystallization and the glass transition temperature. Once again, no correlation was found between the two, which indicates that T_g does not dictate the physical stability of amorphous materials

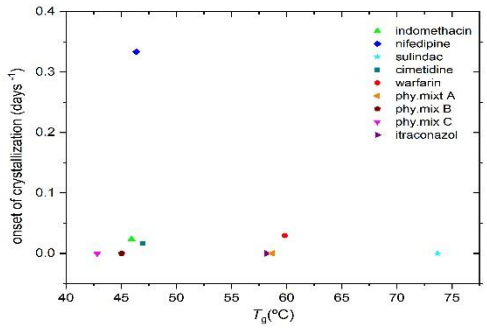

Figure 3.46- Correlation between the onset of crystallization and T_g

3.5.3 Correlation between the onset of crystallization and $\Delta c_p(T_g)$

Since at the glass transition there is a drastic change in the heat capacity of samples, a consequence of the change in molecular dynamics, a possible correlation between this parameter and the onset of crystallization was evaluated. As shown in **Figure 3.47** , no correlation was found.

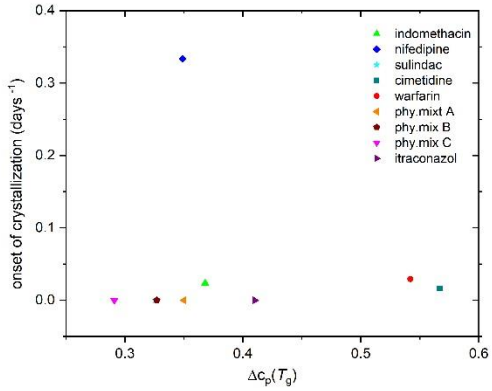

Figure 3.47- Correlation between the onset of crystallization and the $\Delta c_p(T_g)$

3.5.4 Correlation between the onset of crystallization and the fragility index

Since the fragility index is a measure of the susceptibility of structural changes around T_g and of the time scales of molecular motions, the expectation was that this parameter could be related to physical stability. **Figure 3.48** shows that there is no correlation between the fragility index and the onset of crystallization.

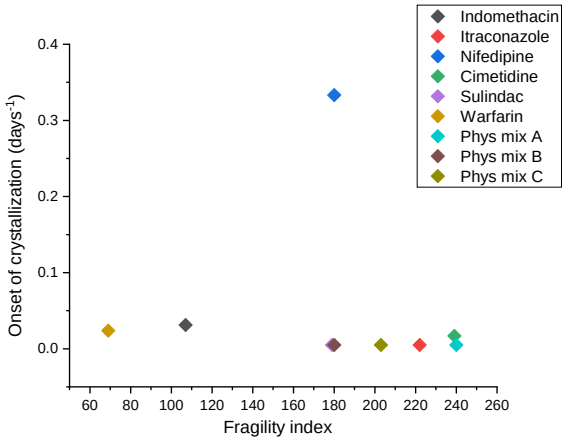

Figure 3.48- Correlation between the onset of crystallization and the fragility index

3.5.5 Correlation between the onset of crystallization and ΔH_{sc-g} at 30ºC

Considering that the amorphous forms are highly energetic, the loss of this excess energy can act like a driving force to the crystallization. Therefore, a possible correlation between the onset of crystallization and the difference in enthalpy between the supercooled liquid and the glass, at the temperature of the stability study, was evaluated. **Figure 3.49**, suggests that there could be a correlation between this excess enthalpy and crystallization since for smaller enthalpy differences between the supercooled liquid and the glass, the chance that complete loss of excess enthalpy will occur in a short time will be greater. However, for a more reliable correlation more values of this excess of enthalpy for other APIs should be included in order to populate the lower enthalpy range.

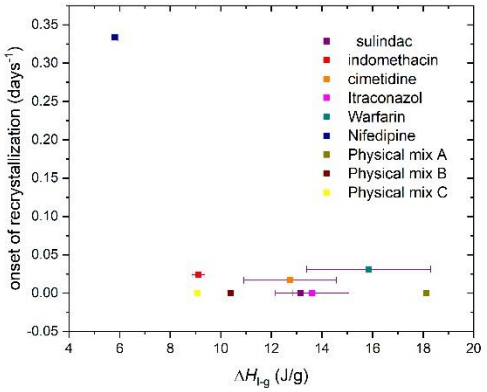

Figure 3.49- Correlation between the onset of crystallization and the excess enthalpy between the supercooled liquid and the glass: APIs (n=3) and ASDs (n=1)

3.5.6 Correlation between the onset of crystallization and T_k

Furthermore, a correlation between the onset of crystallization and the Kauzmann temperature was evaluated. Since T_k corresponds to the temperature at which the liquid exhibits its lowest mobility, it gives an idea of how far the amorphous form is from a state of lowest mobility. According to **Figure 3.50**, apparently, there is no correlation between the onset of crystallization and the Kauzmann temperature.

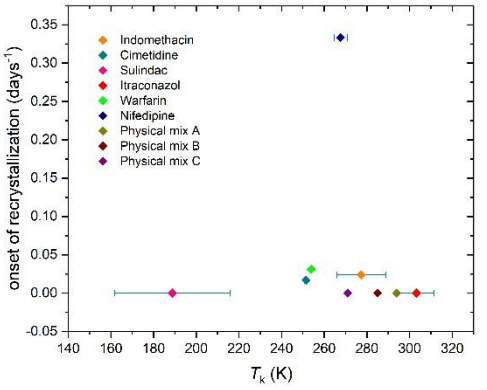

Figure 3.50- Correlation between the onset of crystallization and T_k (API n=3) and ASD (n=1)

3.6 Prediction of the onset of crystallization at 30ºC

As seen in the last subchapter, the enthalpy difference between the supercooled liquid and the glass ($\Delta H_{sc\text{-}g}$) was the parameter that correlated better with the onset of crystallization. Although no clear

correlation was found using the Kauzmann temperature, it made sense that the tendency for crystallization depends on how far the stability temperature is from the temperature at which molecular motions are minimum. Therefore, a new model for prediction of onsets of crystallization was developed, which incorporates kinetics of relaxation but also thermodynamics parameters. The models found in literature are not exactly used for prediction of onsets of crystallization, but only to evaluate the changes in molecular mobility over a range of temperatures (e.g. VTF model) or the kinetics of relaxation (e.g. KWW model [47]). To compare the KWW model with the new model, the onset of crystallization considered for the former is the time that it takes for the glass to relax 99% of the maximum enthalpy. This % was defined for convenience since the KWW model cannot mathematically predict the time for complete relaxation. **Table 3.7** presents the obtained onset of crystallization with the different models

Table 3.7- Comparison between of the onset of crystallization obtained by different models

API	Onset of crystallization (days)		
	Literature model	**New model**	**Stability**
Indomethacin	61464 (±19790)	31 (±3)	32
Nifedipine	185 (±172)	46(±38)	3
Cimetidine	7012 (±9565)	1178 (±1352)	59
Warfarin	204 (±152)	48 (±34)	42
Sulindac	754 (±247)	1064 (±665)	-
Itraconazole	641959 (±320750)	6195543 (±9374303)	-
Physical mix A	7368	10479	-
Physical mix B	1294036	4078	-
Physical mix C	17335	653	-

Comparing the predicted results with the real onsets of crystallization detected during the stability study, it is possible to see that the new model yields onsets of crystallization much closer to the real values. Unfortunately, in the case of cimetidine the results were very different. The reason for such big difference is the fact that, during stability, only one of the cimetidine samples showed signs of crystallinity and consequently, the onset detected should not be representative. Regarding the nifedipine results, the deviation may be related to unusual noise detected in the DSC data. The fact that the standard deviations of the determined values for the onset of crystallization are very significant is owing to the errors and variability associated with the determination of the thermodynamics parameters.

Overall, the literature model predicts onsets of crystallization higher than the new one. The postulation that this time corresponds to a loss of 99% of the maximum enthalpy can lead to some doubts but increasing this loss to 99.9% leads to an increase of this time, as shown in **Table 3.8** .

Table 3.8- Onset of crystallization obtained considering 99.9% of loss of energy

API	Onset of crystallization (days)
Indomethacin	56305(±194338)
Nifedipine	1005 (±1106)
Cimetidine	98467(±136270)
Warfarin	590(±465)
Sulindac	1836(±620)
Itraconazole	3187732(±1620430)
Physical mix.A	27382
Physical mix.B	130395
Physical mix.C	19514886

It must be pointed out that possible discrepancies between real onsets of crystallization and predicted values can be attributed to variability in the preparation technique. Ideally the same cooling rates should be applied to all samples prepared for stability, which was not the case. On the other hand, it is important to assure that the molten sample, prepared in the hot plate, is cooled homogeneously and that the thickness of glass film formed is thin enough so that the heat can be removed totally from the whole sample in a very short time. Since during the experiments the control of these variables was not completely assured these results reflect some variability inherent to the experiments.

4

Conclusions and Future Work

The main goal of this work was not only to understand and evaluate the parameters that govern the physical stability of amorphous APIs and ASDs, but also to develop a predictive model of physical stability, which can be applied in a pre-formulation stage.

The different correlations evaluated showed that, firstly, the glass transition temperature is not the main determinant in the physical stability of amorphous material. Regarding the fragility results, although it was not possible to establish a correct ranking with the determined values, all APIs were classified as fragile. With respect to future work, the determination of this parameter should consider triplicate experiments in order to guarantee more confidence in the results.

The effect of relaxation showed to have influence on the physical stability; however, it cannot be used to predict stability alone. The activation energy around T_g was similar for the different APIs, but in the case of the sub-α relaxations, it was possible to establish a ranking of the molecular mobility as a function of the activation energy values. Lower activation energies lead to higher molecular mobility. As future work, it should be considered that the DRS experiments should be done in triplicates but also, they should be extended for all APIs. Additionally, it should be considered a more complex analysis of these results with different models that explains the relaxation mechanisms.

The model that was developed to predict physical stability considers that the Kauzmann temperature has impact on the physical stability. However, the prediction is not only governed by thermodynamic factors but also kinetics factors, as relaxation occurs with time. The fact that in some cases there was a difference between the onset detected during stability and the onset predicted may be explained by variability associated with the preparation of the amorphous samples. The variability associated with the determination of thermodynamics parameters used showed to have a high impact on the determination of these values, and consequently, on the onset of crystallization. Concerning future work, it should be considered not only a different amorphization procedure but also the preparation of triplicates, in the case of melt-quenching, to be analyzed at the different time points.

Moreover, the employment of this new approach is very advantageous not only because data can be obtained from simple DSC measurements but also because it can provide meaningful information about the recrystallization behavior. Besides these advantages, the new approach saves more time and cost

effective when compared to long term studies but also is an advanced characterization technique that can be used as a screening tool to choose which formulations are more stable.

5

References

[1] J. Wiley, *Pharmaceutical Amorphous Solids Dispersions*. 2015.

[2] Y. Cui, “A material science perspective of pharmaceutical solids,” *Int. J. Pharm.*, vol. 339, no. 1–2, pp. 3–18, 2007.

[3] K. Nanakwani, S. R. Modi, L. Kumar, and A. K. Bansal, “Role of thermodynamic, kinetic and structural factors in the recrystallization behavior of amorphous erythromycin salts,” *Thermochim. Acta*, vol. 582, pp. 77–85, 2014.

[4] J. A. Baird and L. S. Taylor, “Evaluation of amorphous solid dispersion properties using thermal analysis techniques,” *Adv. Drug Deliv. Rev.*, vol. 64, no. 5, pp. 396–421, 2012.

[5] W. L. Chiou and S. Riegelman, “Preparation and dissolution characteristics of several fast-release solid dispersions of griseofulvin,” *J. Pharm. Sci.*, vol. 58, no. 12, pp. 1505–1510, 1969.

[6] S. Greco, J. R. Authelin, C. Leveder, and A. Segalini, “A practical method to predict physical stability of amorphous solid dispersions,” *Pharm. Res.*, vol. 29, no. 10, pp. 2792–2805, 2012.

[7] K. Graeser, J. Patterson, and T. Rades, “Applying Thermodynamic and Kinetic Parameters to Predict the Physical Stability of Two Differently Prepared Amorphous Forms of Simvastatin,” *Curr. Drug Deliv.*, vol. 6, no. 4, pp. 374–382, 2009.

[8] K. A. Graeser, J. E. Patterson, J. A. Zeitler, K. C. Gordon, and T. Rades, “Correlating thermodynamic and kinetic parameters with amorphous stability,” *Eur. J. Pharm. Sci.*, vol. 37, no. 3–4, pp. 492–498, 2009.

[9] D. Mahlin and C. A. S. Bergström, “Early drug development predictions of glass-forming ability and physical stability of drugs,” *Eur. J. Pharm. Sci.*, vol. 49, no. 2, pp. 323–332, 2013.

[10] Y. Huang and W.-G. Dai, “Fundamental aspects of solid dispersion technology for poorly soluble drugs,” *Acta Pharm. Sin. B*, vol. 4, no. 1, pp. 18–25, 2013.

[11] G. Chawla and A. K. Bansal, “Molecular mobility and physical stability of amorphous irbesartan,” *Sci. Pharm.*, vol. 77, no. 3, pp. 695–709, 2009.

[12] Y. Liu, B. Bhandari, and W. Zhou, “Glass transition and enthalpy relaxation of amorphous food saccharides: A review,” *J. Agric. Food Chem.*, vol. 54, no. 16, pp. 5701–5717, 2006.

[13] B. C. Hancock and G. Zografi, “Characteristics and Significance of the Amorphous State in Pharmaceutical Systems,” *J. Pharm. Sci.*, vol. 86, no. 1, pp. 1–12, 2002.

[14] P. J. Skrdla, P. D. Floyd, and P. C. Dell'Orco, "Predicting the solubility enhancement of amorphous drugs and related phenomena using basic thermodynamic principles and semi-empirical kinetic models," *Int. J. Pharm.*, vol. 567, no. May, p. 118465, 2019.

[15] J. C. Dinunzio *et al.*, "Enhancing Polymers for Improved Bioavailability of," *Mol. Pharm.*, vol. 5, no. 6, pp. 968–980, 2008.

[16] D. B. Warren, H. Benameur, C. J. H. Porter, and C. W. Pouton, "Using polymeric precipitation inhibitors to improve the absorption of poorly water-soluble drugs: A mechanistic basis for utility," *J. Drug Target.*, vol. 18, no. 10, pp. 704–731, 2010.

[17] K. A. Graeser, J. E. Patterson, J. A. Zeitler, and T. Rades, "The role of configurational entropy in amorphous systems," *Pharmaceutics*, vol. 2, no. 2, pp. 224–244, 2010.

[18] H. H. Hou *et al.*, "Impact of Method of Preparation of Amorphous Solid Dispersions on Mechanical Properties: Comparison of Coprecipitation and Spray Drying," *J. Pharm. Sci.*, vol. 108, no. 2, pp. 870–879, 2019.

[19] D. D. Le Pevelen and G. E. Tranter, "FT-IR and Raman Spectroscopies, Polymorphism Applications," *Encyclopedia of Spectroscopy and Spectrometry*. Elsevier Ltd., pp. 750–761, 2016.

[20] J. Haleblian and W. McCrone, "Pharmaceutical applications of polymorphism," *J. Pharm. Sci.*, vol. 58, no. 8, pp. 911–929, 1969.

[21] A. Y. Lee, D. Erdemir, and A. S. Myerson, "Crystal Polymorphism in Chemical Process Development," *Annu. Rev. Chem. Biomol. Eng.*, vol. 2, no. 1, pp. 259–280, 2011.

[22] D. Giron, "Thermal analysis characterisation and calorimetric of polymorphs methods in the and solvates," *Thermochim. Acta*, vol. 248, no. 94, pp. 1–59, 1995.

[23] A. Docoslis, K. L. Huszarik, G. Z. Papageorgiou, D. Bikiaris, A. Stergiou, and E. Georgarakis, "Characterization of the distribution, polymorphism, and stability of nimodipine in its solid dispersions in polyethylene glycol by micro-Raman spectroscopy and powder x-ray diffraction," *AAPS J.*, vol. 9, no. 3, pp. E361–E370, 2007.

[24] E. H. Lee, "A practical guide to pharmaceutical polymorph screening & selection," *Asian J. Pharm. Sci.*, vol. 9, no. 4, pp. 163–175, 2014.

[25] L. Almeida E Sousa, S. M. Reutzel-Edens, G. A. Stephenson, and L. S. Taylor, "Assessment of the amorphous 'solubility' of a group of diverse drugs using new experimental and theoretical approaches," *Mol. Pharm.*, vol. 12, no. 2, pp. 484–495, 2015.

[26] P. Atkins and J. Paula de, *Elements of physical chemistry*, no. c. 2009.

[27] S. L. Shamblin, X. Tang, L. Chang, B. C. Hancock, and M. J. Pikal, "Characterization of the time scales of molecular motion in pharmaceutically important glasses," *J. Phys. Chem. B*, vol. 103, no. 20, pp. 4113–4121, 1999.

[28] F. H. Stillinger, "Supercooled liquids, glass transitions, and the Kauzmann paradox," *J. Chem. Phys.*, vol. 88, no. 12, pp. 7818–7825, 1988.

[29] I. M. Hodge, "Adam-Gibbs formulation of enthalpy relaxation near the glass transition," *J. Res. Natl. Inst. Stand. Technol.*, vol. 102, no. 2, p. 195, 1997.

[30] M. Gordon and J. S. Taylor, “Ideal Copolymers and the Second-Order Transitions of Synthetic Rubbers. I. Noncrystalline Copolymers,” *Rubber Chem. Technol.*, vol. 26, no. 2, pp. 323–335, 1953.

[31] E. O. Kissi, H. Grohganz, K. Löbmann, M. T. Ruggiero, J. A. Zeitler, and T. Rades, “Glass-Transition Temperature of the β-Relaxation as the Major Predictive Parameter for Recrystallization of Neat Amorphous Drugs,” *J. Phys. Chem. B*, vol. 122, no. 10, pp. 2803–2808, 2018.

[32] S. Baghel, H. Cathcart, W. Redington, and N. J. O’Reilly, “An investigation into the crystallization tendency/kinetics of amorphous active pharmaceutical ingredients: A case study with dipyridamole and cinnarizine,” *Eur. J. Pharm. Biopharm.*, vol. 104, no. April 2016, pp. 59–71, 2016.

[33] K. Geirhos, P. Lunkenheimer, and A. Loidl, “Johari-Goldstein Relaxation Far Below T g : Experimental Evidence for the Gardner Transition in Structural Glasses ?,” *Phys. Rev. Lett.*, vol. 120, no. 8, p. 85705, 2018.

[34] N. Solids, “Relaxation in liquids, polymers and plastic crystals - strong/fragile patterns and problems,” *J. Non. Cryst. Solids*, vol. 133, no. Part I, pp. 13–31, 1991.

[35] T. Review, “Kinetic and structural fragility — a correlation between structures and dynamics in metallic liquids and glasses,” pp. 0–41, 2017.

[36] C. Yildirim, J. Raty, and M. Micoulaut, “Revealing the role of molecular rigidity on the fragility evolution of glass- forming liquids,” pp. 1–22.

[37] Q. Zheng, J. C. Mauro, and Y. Yue, “Reconciling calorimetric and kinetic fragilities of glass-forming liquids,” *J. Non. Cryst. Solids*, vol. 456, pp. 95–100, 2017.

[38] P. Chakravarty, K. Pandya, and K. Nagapudi, “Determination of Fragility in Organic Small Molecular Glass Forming Liquids: Comparison of Calorimetric and Spectroscopic Data and Commentary on Pharmaceutical Importance,” *Mol. Pharm.*, vol. 15, no. 3, pp. 1248–1257, 2018.

[39] K. F. Kelton, “Kinetic and structural fragility - A correlation between structures and dynamics in metallic liquids and glasses,” *J. Phys. Condens. Matter*, vol. 29, no. 2, pp. 0–41, 2017.

[40] L. Berthier, M. Ozawa, and C. Scalliet, “Configurational entropy of glass-forming liquids,” *J. Chem. Phys.*, vol. 150, no. 16, 2019.

[41] J. C. Dyre, T. Hechsher, and K. Niss, “A brief critique of the Adam-Gibbs entropy model,” *J. Non. Cryst. Solids*, vol. 355, no. 10–12, pp. 624–627, 2009.

[42] G. A. Schwartz, Á. Alegría, and J. Colmenero, “Adam-Gibbs based model to describe the single component dynamics in miscible polymer blends under hydrostatic pressure,” *J. Chem. Phys.*, vol. 127, no. 15, pp. 1–8, 2007.

[43] C. Mao, S. P. Chamarthy, and R. Pinal, “Calorimetric study and modeling of molecular mobility in amorphous organic pharmaceutical compounds using a modified Adam-Gibbs approach,” *J. Phys. Chem. B*, vol. 111, no. 46, pp. 13243–13252, 2007.

[44] S. Page and R. Maurer, *Amorphous Solid Dispersions: Theory and Practice*, vol. 21. Springer, 2014.

[45] Q. Zheng, J. C. Mauro, and Y. Yue, “Reconciling calorimetric and kinetic fragilities of glass-forming liquids,” *J. Non. Cryst. Solids*, pp. 10–15, 2016.

[46] R. R. Nigmatullin, S. I. Osokin, and G. Smith, “New approach in the description of dielectric relaxation

phenomenon: Correct deduction and interpretation of the Vogel-Fulcher-Tamman equation," *J. Phys. Condens. Matter*, vol. 15, no. 20, pp. 3481–3503, 2003.

[47] G. Van Den Mooter, P. Augustijns, and R. Kinget, "Stability prediction of amorphous benzodiazepines by calculation of the mean relaxation time constant using the Williams-Watts decay function," *Eur. J. Pharm. Biopharm.*, vol. 48, no. 1, pp. 43–48, 1999.

[48] A. R. Brás, J. P. Noronha, A. M. Antunes, M. M. Cardoso, M. M. Dionísio, and N. T. Correia, "Molecular motions in amorphous ibuprofen as studied by broadband dielectric spectroscopy," *J. Phys. Chem. B*, vol. 112, no. 35, pp. 11087–11099, 2008.

[49] A. G. Jones, "Crystallization principles and techniques," *Cryst. Process Syst.*, pp. 58–79, 2002.

[50] K. Kawakami, "Nucleation and crystallization of celecoxib glass : Impact of experience of low temperature on physical stability," *Thermochim. Acta*, vol. 671, pp. 43–47, 2019.

[51] H. P. Diogo and J. J. Moura Ramos, "Are crystallization and melting the reverse transformation of each other?," *J. Chem. Educ.*, vol. 83, no. 9, pp. 1389–1392, 2006.

[52] V. Caron, C. Bhugra, and M. J. Pikal, "Prediction of onset of crystallization in amorphous pharmaceutical systems: Phenobarbital, nifedipine/PVP, and phenobarbital/PVP," *J. Pharm. Sci.*, vol. 99, no. 9, pp. 3887–3900, 2010.

[53] A. . Fallis, "Why Modulated DSC®? ; An Overview and Summary of Advantages and Disadvantages Relative to Traditional DSC," *J. Chem. Inf. Model.*, vol. 53, no. 9, pp. 1689–1699, 2013.

[54] TA Instruments, *Thermal Application Note: Purge Gas Recommendations for Use in Modulated DSC*. TA Instruments (Thermal Analysis & Rheology), 2006.

[55] C. Tedesco, *X-ray Powder Diffraction*, Second Edi., vol. 2. Elsevier, 2017.

[56] P. F. Cheng, J. Song, Q. P. Wang, S. T. Li, J. Y. Li, and K. N. Wu, "Fine representation of dielectric properties by impedance spectroscopy," *J. Alloys Compd.*, vol. 740, pp. 36–41, 2018.

[57] F. Kremer and A. Schönhals, *Broadband Dielectric Spectroscopy*. Springer, 2003.

[58] S. U. Shahin Thayyil M, "Fragility of Cimetidine Drug Probed by Broadband Dielectric Spectroscopy," *Transl. Med.*, vol. 04, no. 04, pp. 2013–2015, 2014.

[59] B. Engineering, "Thermodynamic Modeling of Activity Coefficient and Prediction of Solubility: Part 2. Semipredictive or Semiempirical Models," *Online*, vol. 95, no. 4, pp. 798–809, 2006.

[60] H. Bin Yu, W. H. Wang, and K. Samwer, "The β relaxation in metallic glasses: An overview," *Mater. Today*, vol. 16, no. 5, pp. 183–191, 2013.

[61] Z. Wojnarowska *et al.*, "Broadband dielectric relaxation study at ambient and elevated pressure of molecular dynamics of pharmaceutical: indomethacin," *J. Phys. Chem. B*, vol. 113, no. 37, pp. 12536–12545, 2009.

[62] J. Knapik-Kowalczuk, W. Tu, K. Chmiel, M. Rams-Baron, and M. Paluch, "Co-Stabilization of Amorphous Pharmaceuticals - The Case of Nifedipine and Nimodipine," *Mol. Pharm.*, vol. 15, no. 6, pp. 2455–2465, 2018.

[63] S. A. Surwase *et al.*, "Indomethacin: New polymorphs of an old drug," *Mol. Pharm.*, vol. 10, no. 12, pp. 4472–4480, 2013.

A

Appendix A: Characterization by DSC

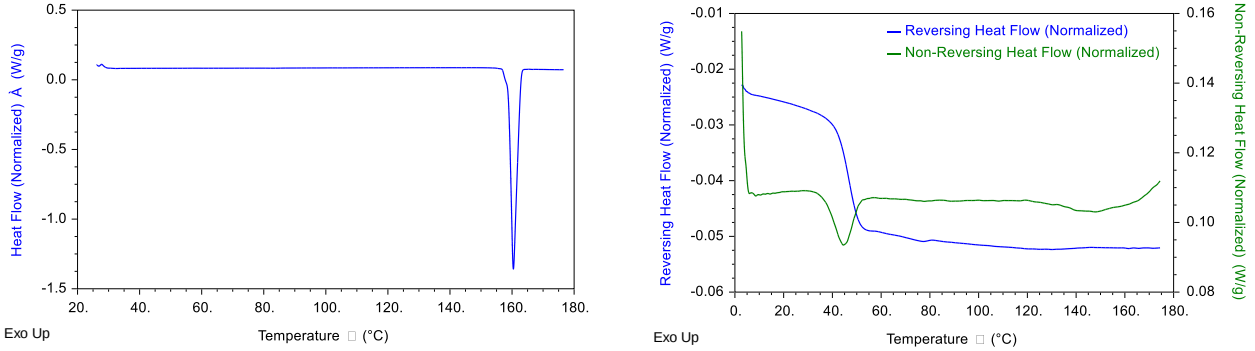

Figure A.6.1- Characterization of indomethacin

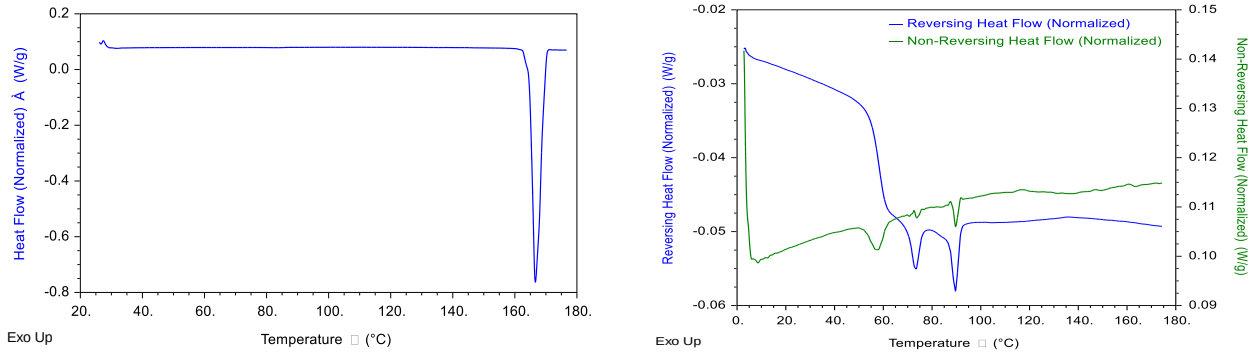

Figure A.6.2- Characterization of itraconazole

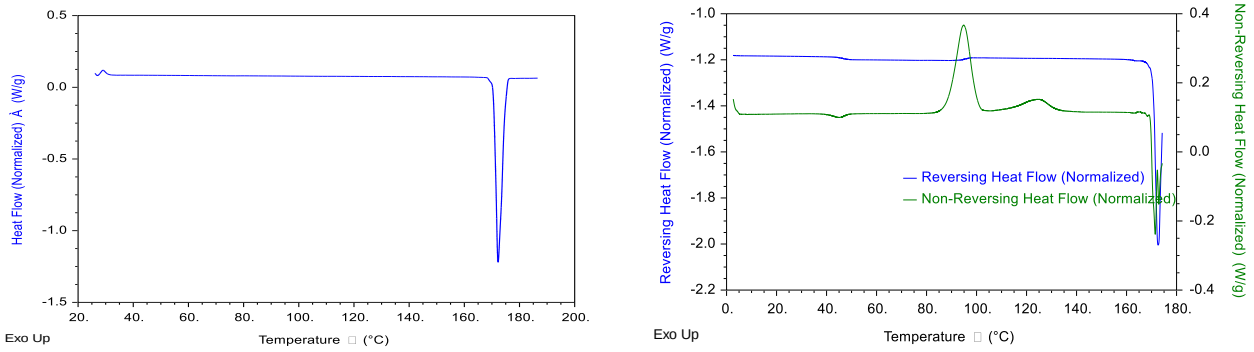

Figure A.6.3- Characterization of nifedipine

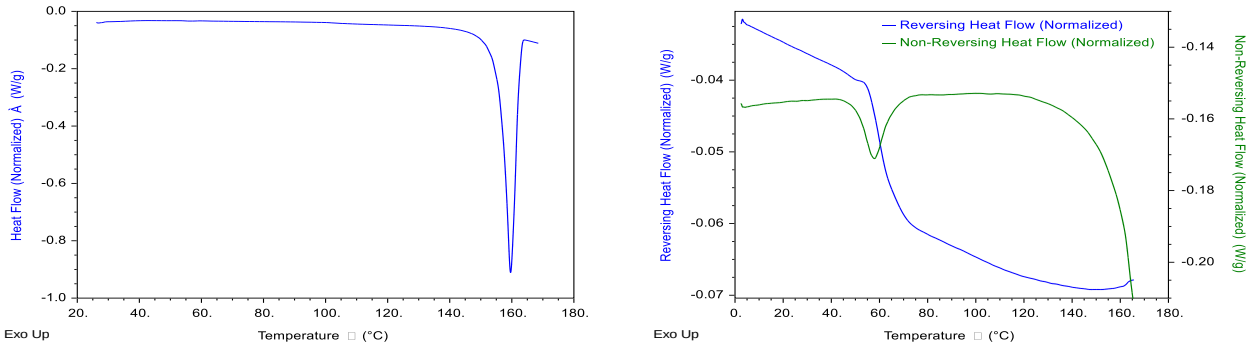

Figure A.6.4- Characterization of warfarin

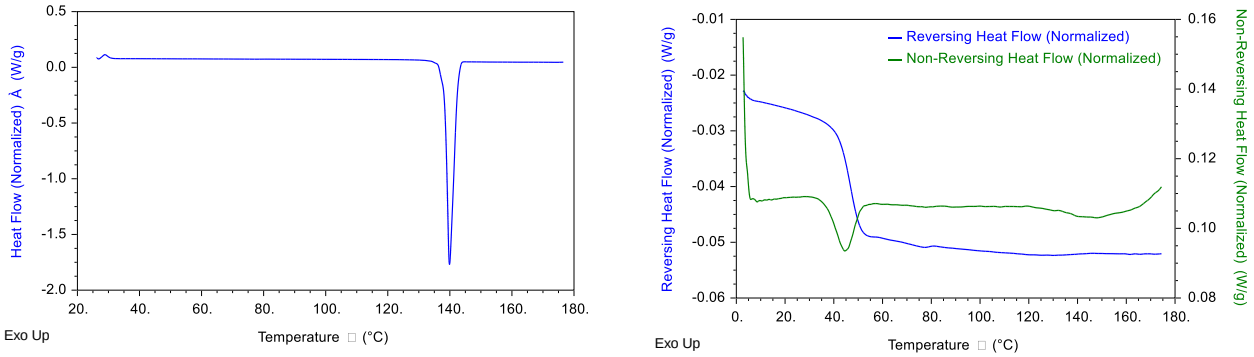

Figure A.6.5- Characterization of cimetidine

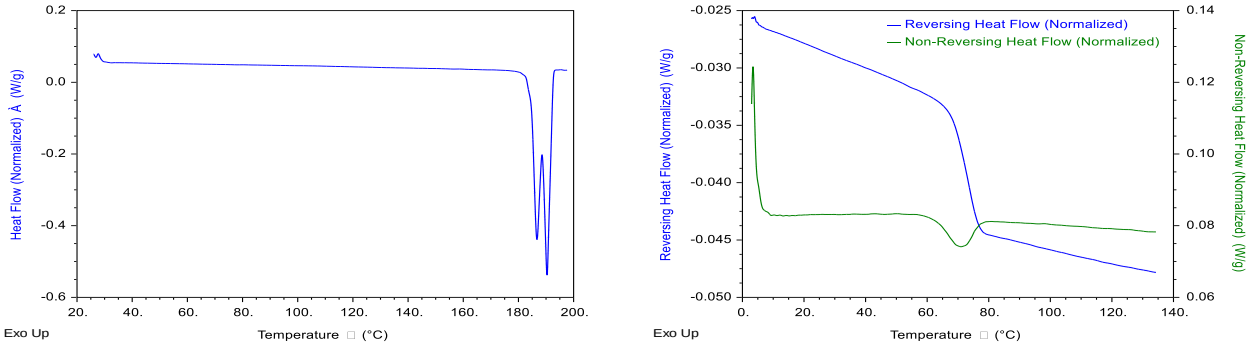

Figure A.6.6- Characterization of sulindac

B

Appendix B: Characterization by XRPD

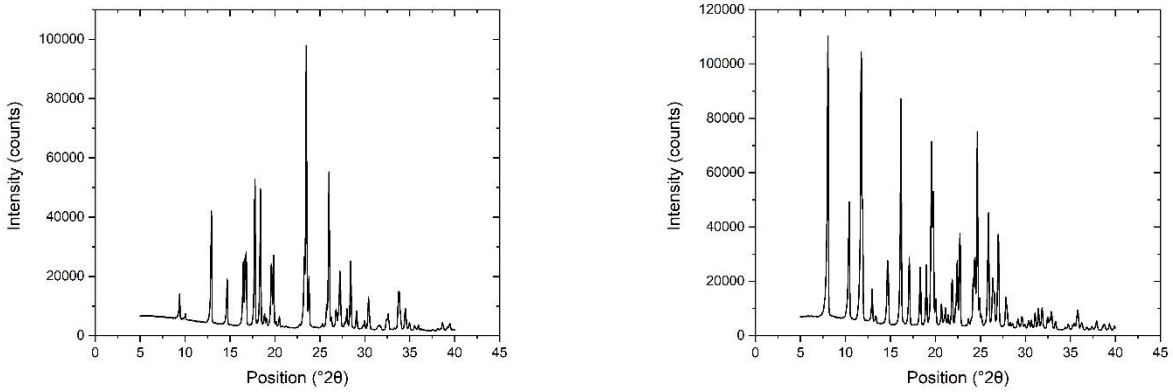

Figure B.7.1- Diffractograms of crystalline cimetidine (left) and nifedipine (right)

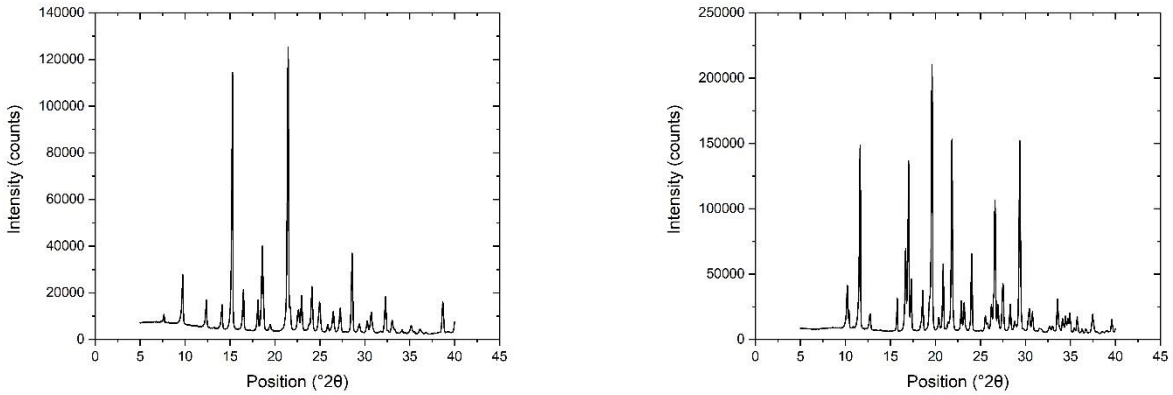

Figure B.7.2- Diffractograms of crystalline sulindac (left) and indomethacin (right)

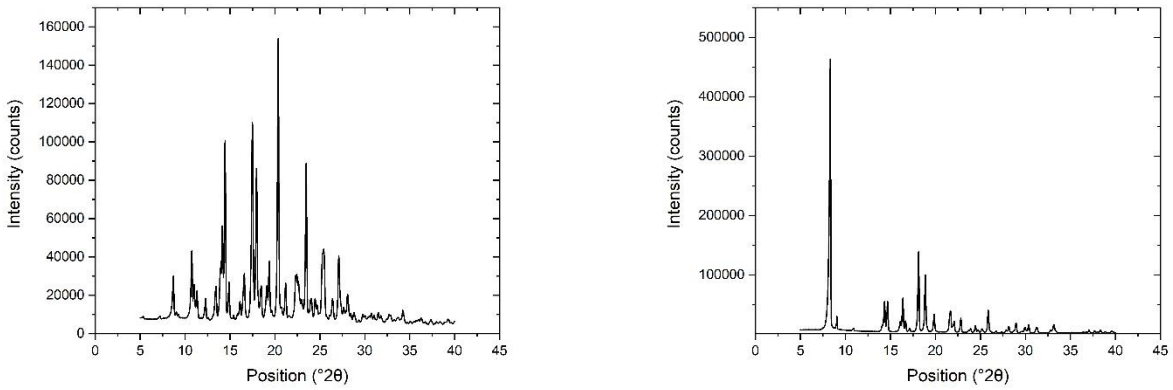

FigureB.7.3- Diffractograms of crystalline itraconazole (left) and warfarin (right)